AD-A183 057 THE EXPERIMENTAL AND ANALYTICAL DEVELOPMENT OF A SENSITIVE SUPERCONDUCTIN..(U) STANFORD UNIV CA DEPT OF PHYSICS W M FAIRBANK 30 OCT 85 AFOSR-TR-87-0924 1/1

UNCLASSIFIED AFOSR-85-0021 F/G 14/2 NL

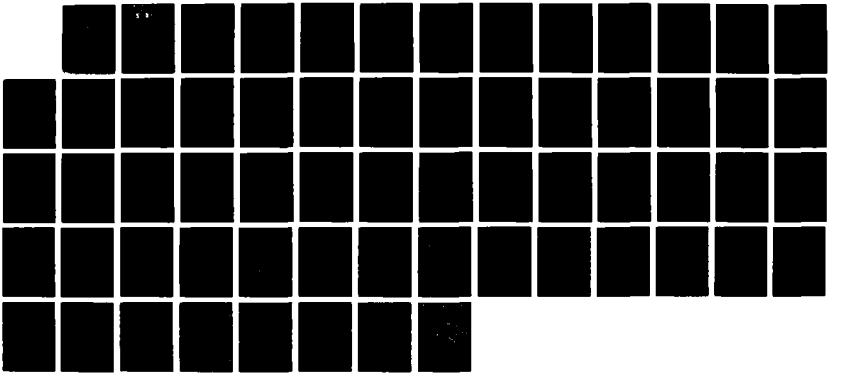

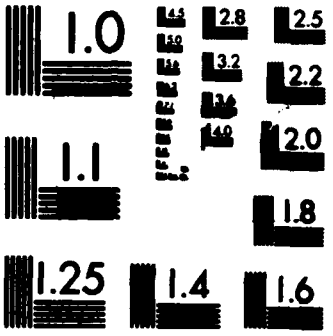

MICROCOPY RESOLUTION TEST CHART
NATIONAL BUREAU OF STANDARDS-1963-A

DTIC FILE COPY

Unclassified

SECURITY CLASSIFICATION OF THIS PAGE

REPORT DOCUMENTATION PAGE

DTIC ELECTE AUG 05 1987 S D

AD-A183 057

1a. REPORT SECURITY CLASSIFICATION: Unclassified	1b. RESTRICTIVE MARKINGS
2a. SECURITY CLASSIFICATION AUTHORITY	3. DISTRIBUTION/AVAILABILITY OF REPORT: Approved for public release, distribution unlimited
2b. DECLASSIFICATION/DOWNGRADING SCHEDULE	
4. PERFORMING ORGANIZATION REPORT NUMBER(S)	5. MONITORING ORGANIZATION REPORT NUMBER(S): AFOSR-TR-87-0924
6a. NAME OF PERFORMING ORGANIZATION: Stanford University	6b. OFFICE SYMBOL (If applicable):
6c. ADDRESS (City, State and ZIP Code): Department of Physics, Standford University, Stanford, CA 94305	7a. NAME OF MONITORING ORGANIZATION: AFOSR
	7b. ADDRESS (City, State and ZIP Code): Building 410, Bolling AFB, Washington D.C. 20332-6448
8a. NAME OF FUNDING/SPONSORING ORGANIZATION: AFOSR	8b. OFFICE SYMBOL (If applicable): NP
	9. PROCUREMENT INSTRUMENT IDENTIFICATION NUMBER: AFOSR-85-0021
8c. ADDRESS (City, State and ZIP Code): Bldg 410, Bolling AFB, Washington D.C. 20332-6448	10. SOURCE OF FUNDING NOS.

PROGRAM ELEMENT NO.	PROJECT NO.	TASK NO.	WORK UNIT NO.
61102F	2301	A8	

11. TITLE (Include Security Classification): "THE EXPERIMENTAL AND ANALYTICAL DEVELOPMENT OF A SENSITIVE SUPERCONDUCTING ACCELEROMETER AND GRAVITY GRADIOMETER"

12. PERSONAL AUTHOR(S): Dr. William M. Fairbank

13a. TYPE OF REPORT	13b. TIME COVERED	14. DATE OF REPORT (Yr., Mo., Day)	15. PAGE COUNT
FINAL	FROM 84/11/01 TO 85/10/30		59

16. SUPPLEMENTARY NOTATION

17. COSATI CODES			18. SUBJECT TERMS (Continue on reverse if necessary and identify by block number)
FIELD	GROUP	SUB. GR.	Superconducting Accelorometer; Gravity Gradiometer, Experiment, Theory

19. ABSTRACT (Continue on reverse if necessary and identify by block number)

A previously developed gravity gradiometer was further developed to become a very sensitive gravitational gradiometer. A passive subtraction of the thermal sensitivity can be accomplished at low frequencies. This subtraction can be extended to higher frequencies by coupling the temperature sensing coil more tightly in temperature to the gradient sensing coil. This could be accomplished by mounting the temperature sensing coil to the inside surface of the gradient sensing coil form.

20. DISTRIBUTION/AVAILABILITY OF ABSTRACT	21. ABSTRACT SECURITY CLASSIFICATION
UNCLASSIFIED/UNLIMITED ☒ SAME AS RPT. ☐ DTIC USERS ☒	UNCLASSIFIED

22a. NAME OF RESPONSIBLE INDIVIDUAL	22b. TELEPHONE NUMBER (Include Area Code)	22c. OFFICE SYMBOL
ROBERT J. BARKER	202/767-5011	NP

DD FORM 1473, 83 APR EDITION OF 1 JAN 73 IS OBSOLETE.

UNCLASSIFIED

SECURITY CLASSIFICATION OF THIS PAGE

87 7 28 412

Department of Physics
Stanford University
Stanford, CA 94305

FINAL REPORT

to the

AIR FORCE OFFICE OF SCIENTIFIC RESEARCH

for

THE EXPERIMENTAL AND ANALYTICAL DEVELOPMENT OF A SENSITIVE SUPERCONDUCTING ACCELEROMETER AND GRAVITY GRADIOMETER

Air Force Contract # AFOSR 85-0021

November 1, 1984 - October 30, 1985

Principal Investigator:
William M. Fairbank
Professor of Physics

FORWARD

Under previous support from the AFOSR, we developed a superconducting accelerometer and gravity gradiometer with the ultimate objective of measuring the inverse square law of gravity. This accelerometer is described in the final report to the AFOSR for Contract # 80-0067. The present report covers a grant of $30,000 to further develop this instrument as a very sensitive gravitational gradiometer. During the past year we worked to improve this gradiometer, and the result of this work is desccribed in the enclosed paper. The work was done primarily by Joel Parke, a visiting graduate student from the University of Maryland, together with his professor, H. J. Paik, who was on sabbatical leave from the University of Maryland.

We have demonstrated that a passive subtraction of the thermal sensitivity can be accomplished at low frequencies. This subtraction can be extended to higher frequencies by coupling the temperature sensing coil more tightly in temperature to the gradient sensing coil. This could be accomplished by mounting the temperature sensing coil to the inside surface of the gradient sensing coil form. This would minimize the thermal time constant between the gradient coil and the temperature coil. It is believed that such a geometry would allow cancellation at frequencies below 0.1 Hz. This combined with conventional temperature stabilization of the inner vacuum can would allow the inverse square law test to be carried out.

Noise in Superconducting Gravity Gradiometers

W. M. Fairbank and E. R. Mapoles
Department of Physics
Stanford University, Stanford, CA 94305

D. DeBra
Department of Aeronautics and Astronautics
Stanford University, Stanford, CA 94305

and

H. J. Paik, J. W. Parke
Department of Physics and Astronomy
University of Maryland, College Park, MD 20742

I. Introduction

In 1974 Long[1] pointed out that existing experimental data allows large violations of the inverse square law of gravity at distances less than 10^3 km. Since Long's initial article appeared in Nature, there has been a great deal of interest in a possible violation of the inverse square law of gravity. Such a possibility is extremely exciting, and may open a door into an area of physics that we have been previously unable to examine.

A recent reanalysis[2] of the Eötvös experiment suggests the existence of a force coupling to Baryon number. The existence of such a force would alter the measurment of the force between two bodies so that the law of gravity would be effectively violated. Any such violation is weaker than the already weak gravitational force, and must compete with a great deal of environmental disturbances of equal or greater strength. Thus, any experiment, designed to detect such a violation, must be extremely sensitive to the forces applied to it and extremly insensitive to environmental changes. These two contradictory requirements have caused experimentalists to attempt to improve the experimental environment and control disturbances.

Recent experiments, using superconducting gravity gradiometers[3,4,5,6] operating at liquid helium temperatures, take advantage of improvements in detection sensitivity and the improved experimental conditions that exist at liquid helium temperatures.

Improvements in detection sensitivity and scale factor stability arise through the unique properties of superconductivity. Superconductivity provides an extremely sensitive superconducting current-to-voltage amplifier, the SQUID. Scale factors are controlled by persistent currents stored in superconducting loops which are absolutely stable.

The experimental conditions that exist at 4 K are vastly superior to those that exist at room temperature. The thermal and mechanical properties of materials are much more stable. The Brownian motion due to the thermal phonon background is also greatly reduced.

Despite these advantages and improvements, superconducting gradiometers still suffer from environmental disturbances. Three main types of disturbances are important. Temperature fluctuations disturb scale factors, change the penetration depth of niobium, and cause mechanical parts to contract and expand. Seismic noise partially couples to the differential modes of the gradiometer. Rotation of the gradiometer introduces centrifugal forces that must be separated from the true gravitational, or at least noninertial, forces acting on the gradiometer. Lastly, magnetic fields can be picked up by the sensing loops in the gradiometer and amplified by the SQUID, introducing additional fictitious signals.

All present superconducting gravity gradiometers suffer from these same noise sources. During 1984 and 1985, we were able to study these noise sources in the Stanford Gravity Gradiometer[4].

At the start of this work, excess noise in the low frequency regime was thought to be due to excess thermal sensitivity in the superconducting readout circuitry. In order to treat and study this effect, a second superconducting readout circuit sensitive only to changes in temperature was added to the gradiometer and coupled to the readout circuit.

By coupling both the gradient sensing coil and the temperature sensing coil to the output SQUID, a passive subtraction of the thermal sensitivity can be accomplished at low frequencies. At the same time, by storing current in only one of the sensing loops, thermal or gravity gradient effects can be independently examined.

The temperature sensing circuit is coupled directly to the gravity gradient sensing circuit through a second transformer. This change in the readout circuit made it necessary to recalibrate the instrument. The analysis for the gradient sensing circuit has been previously done by Mapoles[4] in his thesis. An extension of this analysis, including thermal effects, is presented in Section II.

During the study of the thermal sensitivity of the gradiometer, it was determined that two primary sources of excess noise exist in the gradiometer below 0.2 Hz. These are the large thermal drift in the readout circuit, and the motion of flux trapped in the gradiometer and the surrounding shields.

II. The Basic Gradiometer

The Stanford Gradiometer[4] utilizes a displacement differencing method to detect gravitational gradients. The gradient sensing coil is rigidly attached to one of the proof masses, and measures the distance to the second proof mass. By measuring the relative motion of the two proof masses directly, a partial common mode balance exists before any of the tuning circuits are activated. It is this feature that is the basis of the displacement differencing design.

The gradiometer is shown schematically in Figure 1. All parts are cylindrically symmetric. Each of the two proof masses is supported by two mechanical springs. These mechanical springs are folded cantilevers cut into circular disks of niobium and confine the two proof masses to move along a single axis with a high degree of mechanical compliance.

When a gravitational gradient is applied along the sensitive axis of the gradiometer, the two proof masses move relative to each other. This motion modulates the inductance of the gradient sensing coil which in turn is coupled to the SQUID amplifier which amplifies this small change in current. The gradient sensing coil is mounted on the face of m_1 on a 0.25 cm thick coil form of Macor machinable ceramic. The sensing coil is wound in a single layer on the surface of this coil form. It consists of 400 turns of 0.089 mm diameter niobium wire.

Since the Meissner effect will not allow the magnetic field from the gradient sensing coil to penetrate the second proof mass m_2, the inductance of the gradient sensing coil may be written as

$$L_G = \Lambda_G d_G + \Lambda_G (x_2 - x_1) \quad , \tag{1}$$

where Λ_G is the change in inductance/meter given by $\mu_0 n_G^2 A_G$, n_G =

the number of turns/meter, A_G = the area of the 6.9 cm diameter sensing coil, and d_G = the effective initial separation of the coil from the proof mass m_2. x_1 and x_2 represent displacements of m_1 and m_2, respectively.

In addition to this modulation of the gradient sensing coil inductance by the relative motion of m_1 and m_2, any change in temperature will cause a change in the effective spacing, d_G. This can be represented by a temperature dependent term $\Lambda_{GT}(T-T_0)$ so that L_G is completely described by

$$L_G = \Lambda_G d_G + \Lambda_G(x_2-x_1) + \Lambda_{GT}(T-T_0) , \tag{2}$$

where Λ_{GT} gives the change in inductance/Kelvin, and will be calculated in Section V.

The temperature sensing coil L_T was wound as two solenoidal coils on the outside of the cylindrical casing of the gradiometer. Each coil has a diameter of 11.43 cm, a width of 2.17 cm, and consists of 240 turns of 0.089 mm niobium wire. These coils are held in place by a thin layer of Stycast epoxy, and shielded by a second superconducting niobium shield. Any change in temperature will cause a change in the effective spacing of the coil to the niobium casing. The inductance of the temperature sensing coil can be written as

$$L_T = \Lambda_T d_T + \Lambda_{TT}(T-T_0) , \tag{3}$$

where Λ_{TT} is the change in inductance/Kelvin, d_T is the effective initial separation, and Λ_T is the inductance/meter given by $2\mu_0 n_T^2 A_T$, where n_T = the number of turns/meter of 0.089 mm diameter niobium wire, and A_T = the area of one of the temperature sensing coils. Λ_{TT} will be calculated in Section V.

These sensing coils, for gradient and temperature, are coupled together using two impedance matching transformers, and

connected to the rf SQUID[7] as shown in Figure 2. The final output current containing both gradient and thermal terms is amplified by the SQUID.

The degree of coupling from the gradient sensing is proportional to the magnitude of I_{GO}. Similarly, the coupling from the temperature sensing coil is controlled by I_{TO}. To see this quantitatively, it is necessary to write three flux conservation equations, one for each of the loops in Figure 2. These are

$$(4) \qquad (L_2 + L_G)(I_{GO} + i_G) + M_{23} i = (\Lambda_G d_G + L_2) I_{GO} ,$$

$$(5) \qquad (L_3 + L_5 + L_S) i + M_{23}(I_{GO} + i_G) + M_{45}(I_{TO} + i_T) = M_{23} I_{GO} + M_{45} I_{TO} ,$$

$$(6) \qquad (L_T + L_4)(I_{TO} + i_T) + M_{45} i = (\Lambda_T d_T + L_4) I_{TO} ,$$

where the self-inductances L_i and mutual inductances M_{ij} are defined in Figure 2, and i_G and i_T represent signal currents for gradient and temperature. Substituting Eqs. (2) and (3) into Eqs. (4), (5) and (6), linearizing the equations, and solving for the output current i, we obtain

$$(7) \qquad i = \frac{M_{23} I_{GO} \Lambda_G (x_2 - x_1)}{(\Lambda_G d_G + L_2)(L_3 + L_S + L_T') - M_{23}^2} +$$

$$\left\{ \frac{M_{23} I_{GO} \Lambda_{GT}}{(\Lambda_G d_G + L_2)(L_3 + L_S + L_T') - M_{23}^2} + \right.$$

$$\left. \frac{M_{45} I_{TO} \Lambda_{TT}}{(\Lambda_T d_T + L_4)(L_5 + L_S + L_G') - M_{45}^2} \right\} (T - T_O) ,$$

where L_G' = the effective inductance of the gradient sensing coil,

L_G, as seen through the transformer (L_2, L_3) by the SQUID, which is given by

$$L_G' = L_3 - \frac{M_{23}^2}{(L_2 + \Lambda_G d_G)} , \tag{8}$$

and L_T' = the effective inductance of the temperature sensing coil L_T, as seen through the transformer (L_4, L_5) by the SQUID, which is given by

$$L_T' = L_5 - \frac{M_{45}^2}{(L_4 + \Lambda_T d_T)} . \tag{9}$$

In examining the output current i, a natural separation of the two signals, gradient and thermal, can be seen. If we concentrate on the mechanical motion of the gradiometer, we may simplify Eq. (7). Ignoring thermal effects, we have

$$i = \frac{M_{23} I_{G0} \Lambda_G (x_2 - x_1)}{(\Lambda_G d_G + L_2)(L_3 + L_S + L_T') - M_{23}^2} . \tag{10}$$

A gravitational gradient Γ applied to the gradiometer causes a displacement of the two proof masses which is controlled by the stiffness of the differential spring constant $m\omega_D^2$. Thus

$$|x_2 - x_1| = \frac{b}{\omega_D^2} \Gamma , \tag{11}$$

where ω_D is the differential resonance frequency, and b is the baseline between the two accelerometers.

Thus, when a gradient Γ is applied to the gradiometer, an output current i_Γ is produced:

$$(12) \qquad i_\Gamma = \left\{\frac{b}{\omega_D^2}\right\}\left\{\frac{M_{23} I_{GO} \Lambda_G}{(\Lambda_G d_G + L_2)(L_3 + L_S + L_T') - M_{23}^2}\right\}\Gamma \quad .$$

The SQUID amplifies this small current and produces an output voltage given by

$$(13) \qquad v_\Gamma = R\, i_\Gamma \quad ,$$

where $R = 2 \times 10^5\ \Omega$.

Equation (12) shows only part of the dependence of i_Γ on I_{GO}. As expected, the differential resonance frequency ω_D is dependent on the coupling between the mechanical system and the sensing cicuitry.

A natural measure of this coupling can be given by

$$(14) \qquad \beta = \frac{\omega_D^2 - \omega_0^2}{\omega_D^2} \quad ,$$

where ω_0 is the resonance frequency of the differential mode when the stored current I_{GO} is zero.

In order to calculate the degree of coupling, β, and understand the way in which the sensing current affects the differential resonance frequency, we must look at the reaction forces on the proof masses m_1 and m_2 due to the magnetic pressure from the gradient sensing coil. This force is given by

$$(15) \qquad F_{21} = \frac{B^2}{2\mu_0} A_G = \frac{1}{2} \Lambda_G I_G^2 \simeq \frac{1}{2} \Lambda_G I_{GO}^2 + \Lambda_G i_G I_{GO} \quad ,$$

where i_G may be calculated by solving Eqs. (4), (5), and (6). We have

$$(16) \qquad i_G = \frac{-I_{G0}\Lambda_G(x_2 - x_1)}{(L_2 + \Lambda_G d_G) - M_{23}^2/(L_3 + L_S + L_T')} ,$$

where we have ignored second order terms, and terms dependent on $(T - T_0)$.

Substituting Eq. (16) into Eq. (15), we obtain the force, F_{21}, of the gradient sensing coil on m_2:

$$(17) \qquad F_{21} = F_0 - k_\Sigma (x_2 - x_1) ,$$

where

$$(18a) \qquad F_0 = \tfrac{1}{2}\Lambda_G I_{G0}^2 ,$$

$$(18b) \qquad k_\Sigma = \frac{\Lambda_G^2 I_{G0}}{(L_2 + \Lambda_G d_G) - M_{23}^2/(L_3 + L_S + L_T')} .$$

We can begin to see the dependence of ω_D on the degree of coupling from the gradient sensing coil. The electrical circuit supplies a DC force which tends to separate the two proof masses, and an additional spring constant k_Σ which adds to the mechanical spring constant. Newton's equations of motion for m_1 and m_2 give for the two modes of the gradiometer

$$(19a) \qquad \frac{d^2}{dt^2}(x_2 - x_1) = -\frac{(k + 2k_\Sigma)}{m}(x_2 - x_1) ,$$

$$(19b) \qquad \frac{d^2}{dt^2}(x_2 + x_1) = -\frac{k}{m}\left(1 + \frac{2m}{M}\right)(x_2 + x_1) ,$$

where M = the mass of the gradiometer casing, k is the mechanical spring constant from the folded cantilever springs supporting each of the proof masses, and $m = m_1 = m_2$.

The differential and common mode frequency can be seen from

Eqs. (19) to be

$$\omega_D^2 = \omega_0^2 + \frac{2k_E}{m} \quad , \tag{20a}$$

$$\omega_C^2 = \omega_0^2 \left(1 + \frac{2m}{M}\right) \quad . \tag{20b}$$

To complete the analysis, a dependence of k_E on I_{GO} must be included. This dependence arises through the change in the equilibrium spacing of the gradient sensing coil, d_G, as the magnetic pressure on proof masses m_1 and m_2 increases.

In the Stanford gradiometer, unless the sensing current, I_{GO}, was greater than 4.0 A, the sensing coil and the proof mass m_2 touch. Thus for $I_{GO} > I_{GF} = 4.0$ A, the gradient sensing coil equilibrium spacing, d_G, is given by

$$d_G = d_0 + \frac{\Lambda_G (I_{GO}^2 - I_{GF}^2)}{k} \quad , \tag{21}$$

where d_0 = the effective spacing of the gradient sensing coil when $I_{GO} = I_{GF}$.

Combining Eq. (21) with Eqs. (18) and (20), we may solve for the complete dependence of ω_D^2 on I_{GO}^2:

$$\omega_D^2 = \omega_0^2 + \frac{2 \Lambda_G^2 I_{GO}^2}{m\left\{\Lambda_G d_0 + L_2 + \frac{\Lambda_G^2 (I_{GO}^2 - I_{GF}^2)}{k} - \frac{M_{23}^2}{(L_3 + L_S + L_T')}\right\}} \quad . \tag{22}$$

By setting

$$L_0 = \left\{ \Lambda_G d_0 + L_2 - \frac{M_{23}}{(L_3 + L_S + L_T')} \right\} \quad , \tag{23a}$$

$$\gamma = \frac{\Lambda_G^2}{m L_0 (2\pi)^2} \quad , \tag{23b}$$

Eq. (22) may be written as

$$\omega_D^2 = \omega_0^2 + \frac{(2\pi)^2 2 \gamma I_{GO}^2}{\left\{ 1 + \frac{\gamma (I_{GO}^2 - I_{GF}^2)}{f_0^2} \right\}} \quad . \tag{24}$$

The dependence of ω_D^2 on I_{GO}^2 can now be seen clearly. Initially, while I_{GO}^2 is still small, it is constant at ω_0^2. As I_{GO}^2 increases, ω_D^2 climbs to a constant value of $3\omega_0^2$ for large I_{GO}^2. This implies that the range of coupling, β, is 0 to 2/3.

A plot of the experimental data f_D^2 versus I_{GO}^2 and a fit to Eq. (24) is shown in Figure 3. The numerical fit gives

$$f_{0,exp} = 68.9 \text{ Hz} \quad , \tag{25a}$$

$$\gamma_{exp} = 31.4 \text{ Hz}^2/\text{A}^2 \quad . \tag{25b}$$

From the geometry of the cantilever springs as given by Mapoles[4] and using the classical formula for a bent beam, we have

$$f_0^2 = \frac{3}{4} \frac{E \omega h^3}{m \ell^2} \frac{1}{(2\pi)^2} \quad , \tag{26}$$

where m = 1.07 kg is the mass of each proof mass, ω = 9.55 x 10^{-3}m is the width of each cantilever, h = 7.1 x 10^{-4}m is the

thickness of each cantilever, $\ell = 1.115 \times 10^{-2}$ m is the length of each cantilever, and $E = 126.5 \times 10^{9}$ N/m is the Young's modulus of niobium at 4.2 K. Equation (26) gives

$$f_{0,thy} = 74.4 \text{ Hz} \quad . \tag{27}$$

This is in fair agreement with $f_{0,exp}$. A further check can be obtained by calculating f_0 from the f_C in Eq. (20b). Using $f_{C,exp} = 76.9$ Hz, and M = 6.69 kg, we obtain

$$f_0 = 69.2 \text{ Hz} \; . \tag{28}$$

This is in good agreement with $f_{0,exp}$.

In the previous work with the gradiometer, a f_0 of 60 Hz, and a $I_{GF} = 3.0$ A is reported by Mapoles.[4] The shift in f_0 and in I_{GF} can possibly be accounted for if a shift in the equilibrium position of the springs occurred.

γ may be computed from Eq. (23b) by using $\Lambda_G = 0.79$ H/m, m = 1.07 kg, $d_0 = 250$ μm. $L_2 = 186$ μH, $M_{23} = 22$ μH, $L_3 = 4.9$ μH, $L_S = 2$ μH + 0.6 μH (stray inductance), and $L_T' = 0.7$ μH. This value of L_T' is computed by substituting $L_5 = 0.8$ μH, $M_{45} = 4.4$ μH, $d_T = 19$ μm, $\Lambda_T = 2.48$ H/m, and $L_4 = 43$ μH into Eq. (9). This results in a theoretical value for γ:

$$\gamma_{thy} = 45 \text{ Hz}^2/\text{A}^2 \; . \tag{29}$$

Experimentally, we found a smaller number, $\gamma_{Exp} = 31.4 \text{ Hz}^2/\text{A}^2$, as given in Eq. (25b).

Now that we have a clear understanding of the mode structure of the gradiometer and the superconducting readout circuitry, we are in a position to examine the intrinsic noise of the gradiometer.

II. SQUID Amplifier Noise and Brownian Motion

If the gradiometer is operated in a perfectly quiet environment, i.e., with no seismic noise, no background magnetic field, and no thermal drift, then the theoretical performance of the gradiometer is limited by the SQUID amplifier noise and the noise force coming from the phonon background at 4.2 K.

The SQUID amplifier noise is specified as the equivalent input noise energy in J/Hz at the SQUID input sensing coil L_s:

$$\frac{1}{2} L_s \, i_{N,s}^2 \, df = E_{N,s} \, df \quad , \tag{30}$$

where $E_{N,s} = 5 \times 10^{-29}$ J/Hz.

This effective noise current at the input to the SQUID amplifier is equivalent to a gradient noise, $\Gamma_{N,s}$, acting on the gradiometer. To see this clearly, we may rewrite Eq. (12) using Eqs. (14), (18), and (20):

$$i_\Gamma^2 = \frac{\Gamma^2 \, b^2 \, M_{23}^2 \, \beta^2 \, m^2}{4 I_{GO}^2 (L_3 + L_s + L_T')^2 \, \Lambda_G^2} \quad , \tag{31}$$

where β is the amplifier coupling as defined in Eq. (14). By substituting $i_{N,s}^2$ in place of i_Γ^2, we may solve for the effective gradient noise due to the SQUID amplifier noise:.

$$\Gamma_{N,s}^2 \, df = \frac{8 \Lambda_G^2 I_{GO}^2 (L_3 + L_s + L_T')^2 \, E_{N,s}}{m^2 b^2 M_{23}^2 \beta^2 L_s} \, df \quad . \tag{32}$$

The effective gradient noise due to the phonon background at 4.2 K may be computed from the noise force given by the Nyquist theorem:

$$F_{N,T}^2 \, df = \frac{4 k_B T \omega_D}{Q} \, df \quad . \tag{33}$$

This is equivalent to a gradient noise of

$$\Gamma_{N,T}^2 \, df = \frac{8k_B T\omega_D}{b^2 mQ} \, df \quad . \tag{34}$$

These two sources of gradient noise give a lower bound on the performance of the gradiometer:

$$\Gamma_{N,G}^2 \, df \geq \frac{8\Lambda_G^2 I_{GO}^2 (L_3 + L_S + L_T') \quad E_{N,S}^2}{m^2 b^2 M_{23}^2 \beta^2 L_S} \, df + \frac{8k_B T\omega_D}{b^2 mQ} \, df \quad . \tag{35}$$

In general, it is necessary to minimize this sum as a function of I_{GO}. However, in this case, the amplifier noise is dominant. The Brownian motion noise may be computed by using T = 4.2 K, f_D = 84 Hz, m = 1.07 kg, b = 3.2 cm, $k_B = 1.381 \times 10^{-23}$ J/K, $Q = 5 \times 10^6$:

$$\Gamma_{N,T} = 0.068 \text{ E/Hz}^{1/2} \quad , \tag{36}$$

where 1 E = 1 Eötvös unit = $10^{-9} s^{-2}$ is a unit of gravity gradient. This will be much less than $\Gamma_{N,S}$, and we may minimize $\Gamma_{N,S}$ by itself. This is equivalent to minimizing

$$\frac{I_{GO}}{\beta} \quad . \tag{37}$$

This is a minimum when

$$I_{GO}^2 = \frac{f_0^2}{3\gamma} - \frac{I_{GF}^2}{3} \quad . \tag{38}$$

Using $f_{0,exp}$ = 68.8 Hz and γ_{exp} = 31.4 Hz^2/A^2, we have $I_{GO,opt}$ = 6.71 A or equivalently, using Eq. (24), we find

$$\omega_D^2 = \frac{3}{2} \omega_0^2 \qquad \text{or} \qquad \beta_{opt} = 1/3 \quad . \tag{39}$$

Substituting the optimum current into $\Gamma_{N,S}$ gives

$$(40) \qquad \Gamma_{N,S}^2 \, df = \frac{72\Lambda_G^2 \left(\frac{f_0^2}{3\gamma} - \frac{I_{GF}^2}{3}\right)(L_3 + L_S + L_T')^2 \, E_{N,S}}{m^2 b^2 M_{23}^2 L_S} \, df \quad .$$

Substituting $\gamma_{exp} = 31.4 \ Hz^2/A^2$, $f_{0,exp} = 68.9$ Hz, $L_3 = 4.9 \ \mu H$, $L_S = 2 \ \mu H$, $m = 1.07$ kg, $b = 3.2$ cm, $M_{23} = 22 \ \mu H$, $I_{GF} = 4.0$ A, $E_{N,S} = 5 \times 10^{-29}$ J/Hz, and $\Lambda_G = 0.79$ H/m, we obtain

$$(41) \qquad \Gamma_{N,G} \geq 2.2 \ E/Hz^{1/2} \quad .$$

We may also calculate the scale factor from Eq. (31):

$$(42) \qquad \frac{i_\Gamma}{\Gamma} = \frac{b \, M_{23} \, \beta \, m}{2 I_{opt} (L_3 + L_S + L_T') \, \Lambda_G} \quad .$$

Using Eq. (13) and substituting in numerical factors, we find

$$(43) \qquad \frac{V_\Gamma}{\Gamma} = 0.62 \ \mu V/E \quad .$$

$\Gamma_{N,G}$ is the basic noise of the gradiometer and any additional noise is due to thermal, seismic, or magnetic noise in the experimental environment.

For the original Stanford Gradiometer, with a different transformer, Mapoles[4] reported previously that $\gamma = 70 \ Hz^2/A^2$, $I_{GO,opt} = 4.2$ A, and

$$(44) \qquad \frac{V_\Gamma}{\Gamma} = 1.2 \ \mu V/E \quad \text{or} \quad \Gamma_{N,G} = 1.14 \ E/Hz^{1/2} \quad .$$

This decrease of the gradient-to-voltage scale factor is partially due to the smaller coupling of the new transformer used in the present work. However, it does not seem that the factor of 2

decrease can be accounted for entirely by this. The most likely parameter that has changed over 4 years is the coil spacing d_c. Apparently, d_o has increased from approximately 55 μm to 250 μm. This change may be due to a dust particle, or a partial failure of the epoxy bond that holds the gradient sensing coil to the Macor coil form. Without disassembly, it is impossible to completely determine the cause.

III. Gradiometer Performance

Theoretically, (ignoring environmental noise), the output of the gradiometer should be white noise at the level of 1.4 $\mu V/Hz^{1/2}$ from 0.01 Hz to the peaks due to the resonance of the gradiometer in the common and differential mode. After storing a current close to the optimum, I_{GO} = 6.69 A, in the gradiometer sensing coil and balancing the common mode acceleration out of the differential mode, we obtained the data shown in Figures 4, 5, and 6.

The quietest region occurs just below 1 Hz with a noise of approximately 36 $E/Hz^{1/2}$. This is sixteen times the noise floor due to the amplifier noise alone, and it must have been caused by environmental noise. What is even worse is the climb in noise level below 0.1 Hz since this region is where the inverse square law experiment is to be performed. In the region where one may see the signal from the 3.24×10^3 kg steel cylindrical shell, as it is raised and lowered over the experiment, the noise is approximately 250 $E/Hz^{1/2}$. This level is unacceptably high, and must be due to environmental noise, either large thermal drift or the movement of flux trapped in the cryostat. The various peaks seen in the data are caused by resonances in the vibration isolation used to remove seismic noise from the gradiometer.

IV. Thermal Noise in the Gradiometer

The basic sensitivity of the gradiometer to changes in temperature is shown in Eq. (7). If we concentrate on changes in the output current due to a change in temperature, it appreares that we can simplify Eq. (7) to read

$$(45) \qquad i = (T - T_0) \left\{ \frac{M_{23} I_{GO} \Lambda_{GT}}{(\Lambda_G d_G + L_2)(L_3 + L_S + L_T') - M_{23}^2} \right.$$

$$\left. + \frac{M_{45} I_{TO} \Lambda_{TT}}{(\Lambda_T d_T + L_4)(L_5 + L_S + L_G') - M_{45}^2} \right\} .$$

This is not correct, it is important to realize that the proof masses are free to move in response to any change in the gradiometer sensing current $I_{GO} + i_G$. A change in the gradiometer sensing current produces a force

$$(46) \qquad F_{21} \simeq \Lambda_G i_G I_{GO}$$

which attempts to seperate the proof masses a distance

$$(47) \qquad x_2 - x_1 = \frac{\Lambda_G i_G I_{GO}}{k_m} .$$

Substituting Eq. (47) into Eqs. (4), (5), and (6), linearizing the equations, and solving for the current i, we obtain

$$(48)\quad i = (T - T_0)\left\{(1-\beta)\frac{M_{23} I_{G0} \Lambda_{GT}}{(\Lambda_G d_G + L_2)(L_3 + L_S + L_T') - M_{23}^2}\right.$$

$$\left. + \frac{M_{45} I_{T0} \Lambda_{TT}}{(\Lambda_T d_T + L_4)(L_5 + L_S + L_G'') - M_{45}^2}\right\} .$$

where L_G'' is the effective inductance of the gradient sensing coil, when the proof masses are allowed to move, as seen through the transformer (L_2, L_3) by the SQUID. L_G'' is given by

$$(49)\quad L_G'' = L_3 - \frac{M_{23}^2}{L_2 + \Lambda_G d_G}\,\frac{k}{k + k_E \dfrac{[(L_4 + \Lambda_T d_T)(L_S + L_5 + L_G') - M_{45}^2]}{[(L_4 + \Lambda_T d_T)(L_S + L_5 + L_3) - M_{45}^2]}} .$$

In writing Eq. (48), we have assumed that the temperature of the gradiometer is the same everywhere. This should certainly be true at a low enough frequency. However, we will see that this is not true above approximately 0.01 Hz. A more accurate assumption is that each sensing coil has its own temperature; i.e.,

$$(50)\quad i = \left\{(1-\beta)\frac{M_{23} I_{G0} \Lambda_{GT} (T_G - T_0)}{(\Lambda_G d_G + L_2)(L_3 + L_S + L_T') - M_{23}^2} + \frac{M_{45} I_{T0} \Lambda_{TT} (T_T - T_0)}{(\Lambda_T d_T + L_4)(L_5 + L_S + L_G'')}\right.$$

where T_G and T_T are the temperatures of the gradient sensing coil and the temperature sensing coil, respectively.

In examining Eq. (48), is seems clear that the thermal

sensitivity of the gradiometer may be "dropped out" by a correct adjustment of the temperature sensing current, I_{TO}, as a function of I_{GO}. However, Eq. (50) shows that this cancellation will occur only at sufficiently low frequencies where $T_C \approx T_T$. At higher frequencies, a complicated thermal structure will be seen.

At the start of this work, it was felt that the difference in temperature throughout the gradiometer should be negligible below a frequency of approximately 0.1 Hz. We have seen in the experiment, however, that the relevant time scale is on the order of 100 s. Below 0.01 Hz, Eq. (48) starts to approximate the thermal situation in the gradiometer reasonably well.

Indeed, the time scales for thermal heat pulses to move within the gradiometer are on the order of 10 s; however, the phase shift is still apparent at 100 s. This is because thermal systems are first order in nature.

The gradiometer can be broken up into several isolated thermal pieces. Heat first reaches the outside casing (at T_C with a heat capacity C_C), then passes to the bulk of the gradiometer (at T_B with heat capacity C_B). From the bulk of the gradiometer, heat moves slowly through the thin niobium springs to the two proof masses m_1 and m_2 (at T_M with heat capacity C_M), and finally heat moves slowly through the Macor coil form to the gradient sensing coil (at T_M with heat capacity C_G). This is schematically represented in Figure 7.

The thermal equations of "motion" can be written as

(51a)
$$\frac{dT_C}{dt} = \frac{P(t)}{C_C} - \frac{(T_C - T_B)}{\tau_{CB}} \quad ,$$

(51b)
$$\frac{dT_B}{dt} = - \frac{(T_B - T_C)}{\tau_{CB}} \frac{C_C}{C_B} - \frac{(T_B - T_M)}{\tau_{BM}} \frac{C_M}{C_B} \quad ,$$

(51c) $$\frac{dT_M}{dt} = -\frac{(T_M - T_B)}{\tau_{BM}} \quad ,$$

(51d) $$\frac{dT_G}{dt} = -\frac{(T_G - T_M)}{\tau_{MG}} \quad ,$$

where P(t) is heat applied to the outside casing and τ_{ij} is the time constant for heat transfer from the i-th part to the j-th part.

Using this model, and applying a heat impulse to the outside casing through a heater coil, we obtained the parameters given in Table 1. Typical data and fit to the model are shown in Figures 8 and 9.

A partial verification of these parameters may be obtained by examining C_C/C_B and C_M/C_B with an exchange gas pressure approximately 10^{-3} μ.

Since heat capacity is proportional to mass,

(52) $$\frac{C_M}{C_B + C_C} = \frac{m_1 + m_2}{m_C + m_B} = \frac{1.07\ kg + 1.07\ kg}{6.69\ Kg} = 0.32 \quad .$$

Similarly from Table 1,

(53) $$\frac{C_M}{C_B + C_C} = \frac{C_M/C_B}{1 + C_C/C_B} = 0.35 \quad .$$

These numbers are in good agreement.

Using the thermal model of the gradiometer and looking at the steady state response, we may compute the transfer function:

(54) $$\frac{T_C - T_G}{T_C} \quad .$$

This transfer function will tell us the degree of balance between the temperature at the outside case and the temperature at the gradient sensing coil. Setting $P(t)/C_C = A\, e^{st}$ and solving for the steady state response, we obtain

(55) $$\frac{T_C - T_G}{T_C}(s) =$$

$$\frac{s\left\{C_B\tau_{BM}\tau_{CB}\tau_{MG}s^2 + s\left[\tau_{CB}\tau_{MG}(C_M + C_B) + \tau_{BM}(\tau_{MG}C_C + \tau_{CB}C_B)\right] + C_C(\tau_{BM} + \tau_{MG}) + (C_M + C_B)\tau_{CB}\right\}}{(s\tau_{MG} + 1)\left\{C_B\tau_{BM}\tau_{CB}s^2 + \left[\tau_{CB}(C_M + C_B) + \tau_{BM}C_C\right]s + C_C\right\}} \quad .$$

This transfer function is plotted in Figure 10 for the data with approximately $10^{-3}\mu$ exchange gas. It is clear from the plot that the temperature of the outside casing and the temperature of the gradient sensing coil are very different above 0.01 Hz and no temperature balance is possible above this point.

With a little thought, it also becomes clear that the temperature of the gradient sensing coil fluctuates much less than the temperature of the case. At high frequencies, say above 0.2 Hz, all of the thermal noise reaching the case should be much suppressed when it reaches the gradient sensing coil. Quantitatively, if we examine the transfer function

$$(56)\quad \frac{T_G}{T_C}(s) = \frac{1}{\left\{ s^3 \tau_{BM}\tau_{CB}\tau_{MG}\frac{C_B}{C_C} + s^2\left[\tau_{CB}\frac{C_B}{C_C}(\tau_{BM}+\tau_{MG}) + \frac{C_B}{C_C}\frac{C_M}{C_B}\tau_{CB}\tau_{MG}+\tau_{BM}\tau_{MG}\right] + s\left[\tau_{BM}+\tau_{MG}+\tau_{CB}\left(\frac{C_M}{C_B}\frac{C_B}{C_C}+\frac{C_B}{C_C}\right)\right]+1\right\}},$$

it is clear that the gradiometer sensing coil is well filtered by this third order low-pass function. Substituting in the parameters from Table 1 for an exchange gas pressure of approximately $10^{-3}\mu$, we obtain

$$(57)\quad \frac{T_G}{T_C} = \frac{1}{-jf^3(19s)^3 - f^2(46s)^2 + jf(91s)+1},$$

where we have set $s = 2\pi jf$. At a frequency of 0.01 Hz, the difference between T_G and T_C is only 1.6 db. However, at 0.1 Hz, T_G fluctuations are suppressed by 26 db. This increases to 39 db at 0.2 Hz. Clearly, thermal fluctuations should make no contribution to environmental noise in the gradiometer above 0.2 Hz. This is our first indication that the excess noise in the gradiometer may be due to another source.

By storing currents, $I_{TO} = 4.02$ A and $I_{GO} = 0$ A, in the gradiometer, we can magnify thermal noise and suppress inertial disturbances. This data is plotted in Figure 11.

Comparing this with our previous data in Figure 5, we see that our excess noise above 0.2 Hz must be related to inertial disturbances. This comparison is shown more clearly in Figure 12.

Below 0.2 Hz, the excess noise may be due to the movement of magnetic flux trappped in the shields surrounding the gradiometer,

or due to fluctuations in temperature. Inertial disturbances should be somewhat suppressed below 0.2 Hz since, in this region, seismic disturbances drop in amplitude and there are no resonance peaks in the gradiometer suspension structure. This drop in amplitude, which is measured with a room temperature accelerometer constructed at the University of Maryland, is shown in Figure 13. At worst, the seismic noise should provide a flat background, and yet we observe a sharp increase as f becomes zero.

If we examine the output of the gradiometer without any current stored in the readout circuitry, we obtained the data in Figure 14. We observe a large amount of excess noise. This noise cannot be caused by temperature changes in the gradiometer, as the amount of residual current trapped in the gradiometer is very small. Typical data for the gradiometer ouput voltage, with no current stored, is plotted as a function of time, is shown in Figure 15. Flux movement is shown clearly in Figure 15.

The type of step function, as shown in Figure 15, will produce noise with a $1/f^{\alpha}$ characteristic when it is spectrally decomposed. This noise will contribute to the excess noise in the gradiometer below 0.2 Hz. By comparing the data in Figures 14 and 11, we conclude that, while the movement of flux is important, it is not the major source of noise below 0.2 Hz. Adding a μ-metal shield to the dewar would eliminate the low frequency noise due to the movement of trapped flux, but excess thermal noise would still be present. The flux noise is, however, very important in any experiment in which the signal frequency lies above 0.1 Hz.

Mapoles[4] previously reported a thermal sensitivity of the gradiometer, dV/dT, equal to 31.6 x (I_{GO}/1 A) V/K . This is an extraordinary sensitivity to temperature changes. If the gradiometer has 6.69 A stored in the gradient sensing coil, it is necessary to stabilize the temperature to better than 6.6 nK/Hz $^{1/2}$, over the region of experimental interest, in order to

limit the contribution of thermal noise to the total noise so that the SQUID amplifier noise dominates.

By adding the readout circuit sensitive only to changes in temperature, it was hoped that a passive subtraction of temperature changes could be attained for frequencies below 0.1 Hz. We found that this subtraction did not occur until approximately 1 mHz. At this frequency, we did observe much improvement in the thermal sensitivity of the gradiometer.

V. Thermal Sensitivity in the Gradiometer

During the original work on the Stanford Gradiometer, the only candidate for the mechanism that produces the high thermal sensitivity of gradiometer , dV/dT, was the change in the penetration depth of niobium as a function of temperature. This effect was 10 times too small, and the actual mechanism was unknown. Whatever the mechanism, it was thought that it should decrease as the temperature was lowered below 4.2 K. Mapoles constructed a cold plate in order to cool the gradiometer. This did not, however, improve the thermal performance.

We now know that three major mechanisms affect the thermal sensitivity of the gradiometer. These are, the change in penetration depth of niobium, the thermal expansion of Stycast epoxy at cryogenic temperatures, and the change in Young's modulus of niobium below the superconducting transition point.

For the first effect, Mapoles[4] reports that

$$\frac{d\lambda(T)}{dT} = \frac{2\lambda_0}{T_c}\left(\frac{T}{T_c}\right)^3 \left[\, 1 - \left(\frac{T}{T_c}\right)^4 \,\right]^{-3/2} , \tag{58}$$

where λ_0 = 440 Å and T_c = 9.2 K for niobium. At 4.5 K,

$$\frac{d\lambda(T)}{dT} = 1.22 \times 10^{-9} \text{ m/K} . \tag{59}$$

It is difficult to determine the thermal expansion coefficient of Stycast epoxy at 4.5 K, but an estimate may be obtained from Serafini and Koenig[8] of

$$\frac{1}{L}\frac{dL}{dT} \simeq 1.5 \times 10^{-5} \text{ /K} . \tag{60}$$

The change in Young's modulus of niobium as reported by Kramer and Bauer[9] is dependent on the degree of stress in the sample, the degree of chemical purity, and the frequency at which it is measured. A rough estimate of this appears to be

$$\frac{1}{Y}\frac{dY}{dT} = 25 \times 10^{-6}\ /K \quad \text{at 4.5 K}\ , \tag{61a}$$

$$\frac{1}{Y}\frac{dY}{dT} = 50 \times 10^{-6}\ /K \quad \text{at 3 K and below}\ . \tag{61b}$$

These three effects can be used to compute the expected change in self-inductance of the gradient sensing coil and the temperature sensing coil.

The temperature sensing coil is shown schematically in Figure 16. The thickness of the layer of epoxy bonding the niobium wire to the niobium casing of the gradiometer is approximately 130 μm. If we assume that the wire moves half the distance that the epoxy expands or contracts, then the change in the coil spacing may be computed as

$$\left[\frac{d\ d_T}{dT}\right]_{epoxy} = 65\ \mu m \times \frac{1}{L}\frac{dL}{dT} = 0.98 \times 10^{-9}\ m/K\ . \tag{62}$$

The change in the penetration depth of niobium contributes twice, once at the surface of the wire and again at the surface of the casing. There arises, however, a factor of one half which cancels this. The pentration depth is defined as the mean distance over which the magnetic field B penetrates a superconductor. If B_0 is the field strength at the surface and B(x) is the field strength inside the superconductor, then

(63) $$B(x) = B_0 e^{-x/\lambda(T)} \quad .$$

The amount of magnetic energy that penetrates the inside of the superconductor per unit area is equal to

(64) $$\int_0^\infty \frac{B(x)^2}{2\mu_0}\, dx = \int_0^\infty \frac{1}{2\mu_0} B_0^2\, e^{-2x/\lambda(T)}\, dx = \frac{B_0^2}{2\mu_0} \frac{\lambda(T)}{2} \quad .$$

The resulting change in self-inductance effectively modifies d_T as

(65) $$\left[\frac{d\ d_T}{dT}\right]_{penetration} = 2 \times \frac{1}{2} \times \frac{d\lambda(T)}{dT} = 1.2 \times 10^{-9}\ m/K \quad .$$

The change in d_T due to penetration depth changes and thermal expansion add together to give

(66) $$\left[\frac{d\ d_T}{dT}\right]_{total} = 2.2 \times 10^{-9}\ m/K \quad .$$

Λ_{TT} can now be computed by setting

(67) $$\Lambda_{TT} = \Lambda_T \times \left[\frac{d\ d_T}{dT}\right]_{total} = 2.49\ H/m \times 2.2 \times 10^{-9}\ m/K = 5.5\ nH/K \quad .$$

The gradient sensing coil is shown schematically in Figure 17. The sensing coil is held to the Macor coil form by a thin layer of Stycast epoxy approximately 125 μm thick. This Macor coil form is held to the proof mass m_2 by a second layer of Stycast epoxy approximately 25 μm thick.

Because the thermal expansion of the epoxy moves the sensing coil and the coil form towards the proof mass m_1, the equilibrium spacing d_G is reduced. As previously, we assume that the niobium sensing coil moves half as much as the expansion of the epoxy bonding it to the coil form. To this is added the expansion of the thin layer bonding the coil form to the proof mass m_2. The expansion of epoxy gives,

$$(68) \quad \left[\frac{d\, d_G}{dT}\right]_{epoxy} = -(65\ \mu m + 25\ \mu m) \times \frac{1}{L}\frac{dL}{dT} = -1.4 \times 10^{-9}\ m/K \quad .$$

The change in d_G due to penetration depth changes is identical to the change in d_T,

$$(69) \quad \left[\frac{d\, d_G}{dT}\right]_{penetration} = 2 \times \frac{1}{2} \times \frac{d\lambda(T)}{dT} = +1.2 \times 10^{-9}\ m/K \quad .$$

At this point, we immediately notice that Eqs. (64) and (65) almost cancel each other. Thus, without a third mechanism to provide additional thermal sensitivity, there is no hope of explaning the large thermal sensitivity of the gradiometer.

This third mechanism is provided by the niobium springs that support the proof masses. Because the Young's modulus changes as a function of temperature, the equilibrium spacing d_G fluctuates with temperature.

The sensitivity of the gradiometer output to this change is directly proportional to how much the springs are loaded. To see this clearly, we may compute the equilibrium spacing of the two proof masses. The magnetic force causing the masses to separate is

(70) $$\frac{B^2}{2\mu_0} A_G = \frac{1}{2} \Lambda_G I_{GO}^2 \quad .$$

This defines the equilibrium stretch d_{ST}. Setting the restoring force equal to the magnetic force, we obtain

(71) $$k_M \frac{d_{ST}}{2} = \frac{1}{2} \Lambda_G I_{GO}^2 \quad ,$$

where the factor of 2 enters because both proof masses move. Solving for d_{ST}, we find

(72) $$d_{ST} = \frac{\Lambda_G I_{GO}^2}{k} \quad .$$

The mechanical spring constant k is directly proportional to the Young's modulus of niobium. Differentiating d_G with respect to temperature, using Eq. (25) and setting $k = m\omega_0^2$, we find

(73) $$\left[\frac{d\ d_{ST}}{dT}\right]_{spring} = - \frac{\Lambda_G I_{GO}^2}{m\omega_0^2} \frac{1}{Y} \frac{dY}{dT} = \left[\frac{d\ d_G}{dT}\right]_{spring} .$$

Setting Λ_G = 0.79 H/m, m = 1.07 kg, $f_{0,exp}$ = 68.9 Hz, $I_{GO,opt}$ = 6.69 A, and using Eqs. (61) , we obtain:

(74a) $$\left[\frac{d\ d_G}{dT}\right]_{spring} = - 4.4 \times 10^{-9} \text{ m/K} \quad \text{at 4.5 K} \quad ,$$

(74b) $$\left[\frac{d\ d_G}{dT}\right]_{spring} = - 8.8 \times 10^{-9} \text{ m/K at 3 K and below} \quad .$$

In contrast to the change in penetration depth, this effect is much larger at 3 K than at 4.5 K.

Equations (68), (69), and (74) combine to give

$$\left[\frac{d\ d_G}{dT}\right]_{total} = -\ 4.6 \times 10^{-9}\ \text{m/K} \quad \text{at 4.5 K} \quad , \tag{75a}$$

$$\left[\frac{d\ d_G}{dT}\right]_{total} = -\ 9.0 \times 10^{-9}\ \text{m/K at 3 K and below} \quad . \tag{75b}$$

Λ_{GT} can now be computed by setting

$$\Lambda_{GT} = \Lambda_G \times \left[\frac{d\ d_G}{dT}\right]_{total} \quad , \tag{76}$$

substituting in Eqs. (75) and setting $\Lambda_G = 0.79$ H/m, we obtain

$$\Lambda_{GT} = -\ 3.6\ \text{nH/K} \quad \text{at 4.5 K} \quad , \tag{77a}$$

$$\Lambda_{GT} = -\ 7.1\ \text{nH/K} \quad \text{at 3 K and below.} \tag{77b}$$

di/dT for the gradiometer may now be computed. Differentiating Eq. (48) with respect to the gradient sensing coil temperature and the temperature sensing coil temperature, we obtain

$$\frac{1}{I_{Go}} \frac{di}{dT_G} = (1-\beta)\ \frac{M_{23}\Lambda_{GT}}{(\Lambda_G d_G + L_2)(L_3 + L_S + L_T') - M_{23}^2} \quad , \tag{78a}$$

(78b) $$\frac{1}{I_{To}}\frac{di}{dT_T} = \frac{M_{45}\Lambda_{TT}}{(\Lambda_T d_T + L_4)(L_5 + L_3 + L_G'') - M_{45}^2} \quad .$$

By Substituting, Eqs. (67) and (77), and other numerical parameters into these equations, we obtain

(79a) $$\frac{1}{I_{Go}}\frac{di}{dT_G} = 2.0 \times 10^{-5}\ /K \quad \text{at } 4.5\ K \quad ,$$

(79b) $$\frac{1}{I_{Go}}\frac{di}{dT_G} = 4.0 \times 10^{-5}\ /K \quad \text{at } 3\ K \text{ and below} \quad ,$$

(80) $$\frac{1}{I_{To}}\frac{di}{dT_T} = 3.7 \times 10^{-5}\ /K \quad \text{at } 4.5\ K \quad .$$

Using Eq. (13), we can calculate the corresponding change in output voltage:

(81a) $$\left[\frac{dV}{dT_G}\right]_{thy} = R\,\frac{1}{I_{Go}}\frac{di}{dT_G} = 4.0\ V/K \quad \text{at } 4.5\ K \quad ,$$

(81b) $$\left[\frac{dV}{dT_G}\right]_{thy} = R\,\frac{1}{I_{Go}}\frac{di}{dT_G} = 8.0\ V/K \text{ at } 3\ K \quad ,$$

(82) $$\left[\frac{dV}{dT_T}\right]_{thy} = R\,\frac{1}{I_{TO}}\,\frac{di}{dT_T} = 7.4\ \text{V/K} \quad \text{at } 4.5\ \text{K} \quad .$$

Experimentally, we found

(83a) $$\left[\frac{dV}{dT_G}\right]_{exp} = 30.0\ \text{V/K} \quad \text{at } 4.5\ \text{K} \ ,$$

(84) $$\left[\frac{dV}{dT_T}\right]_{exp} = 17.5\ \text{V/K} \quad \text{at } 4.5\ \text{K} \ .$$

Mapoles measured previously

(83b) $$\left[\frac{dV}{dT_G}\right]_{exp} = 43.6\ \text{V/K at } 2.4\ \text{K} \quad .$$

Comparing Eqs. (84) and (82), we find that the experimental value is twice as large as the theoretical value, and our rough estimate for the expansion of stycast epoxy at 4.5K must be too small by a factor of two.

Comparing Eqs. (83) and (81) we find that the experimental value is much larger than the theoretical value. The change in Young's modulus ,as reported by Kramer and Bauer[9], is strongly dependent on the chemical purity and the degree of stress in the sample. It is also dependent on the frequency at which it is

measured. Kramer and Bauer[9] report dY/dT for 80 kHz and 240 kHz. The value at 240 kHz is approximately half as large as that at 80 kHz. Perhaps it is reasonable to suspect that dY/dT is 2 to 3 times larger at 70 Hz. If we substitute

$$\frac{1}{Y}\frac{dY}{dT} = 75 \times 10^{-6} \text{ /K at 4.5 K} , \tag{85}$$

and use a thermal expansion coefficent for stycast epoxy that is twice as large, i.e. ,

$$\frac{1}{L}\frac{dL}{dT} \simeq 3.0 \times 10^{-5} \text{ /K} , \tag{86}$$

we obtain:

$$\left[\frac{dV}{dT_G}\right]_{thy} = 12.7 \text{ V/K at 4.5 K.} \tag{87}$$

This is still too small.

Experimentally, dV/dT_G increases below 3.0 K. This is evidence that our understanding of the thermal properties of the gradiometer is basically correct.

VI. Conclusion

At the start of this work, excess noise in the low frequency regime was thought to be due to excess sensitivity to thermal drift in the gradient sensing circuit. We have confirmed this for frequecies below 0.2 Hz. At higher frequencies, we have shown that there should be no contribution from thermal drift.

Previously the large sensitivity of the gradiometer to thermal drift was not understood. We now understand that this is primarily due to change in Young's modulus of niobium with temperature.

In addition to the noise generated by the thermal drift at low frequencies, we have also found that the motion of flux trapped in the lead shield surrounding the gradiometer leads to noise with a $1/f^{\alpha}$ characteristic. The addition of a μ-metal shield to the cryostat would remove this.

We have demonstrated that a passive subtraction of the thermal sensitivity can be accomplished at low frequencies. This subtraction can be extended to higher frequencies by coupling the temperature sensing coil more tightly thermally to the gradient sensing coil. This could be accomplished by mounting the temperature sensing coil to the inside surface of the gradient sensing coil form. This would minimize the thermal time constant between the gradient coil and the temperature coil. It is believed that such a geometry would allow cancellation at frequencies below 0.1 Hz. This combined with conventional temperature stabilization of the inner vacuum can would allow the inverse square law test to be carried out.

Another way of reducing the temperature sensitivity of the Stanford Gradiometer is using a current-differencing scheme employed in the gradiometer developed at the University of Mayland[6]. In this device, the displacements of the two proof masses are sensed by two

separate sensing coils, each mounted on the same side of the respective proff mass. A temperature change now produces effects which look like a commmon acceleration and are therefore rejected by the common mode balance of the two sensing loops.

Acknowledgement

We wish to acknowledge the valuable contributions by Dr. Mike McAshan.

REFERENCES

1. D. R. Long, Nature 260, 417 (1976).
2. E. Fishbasch, D. Sudarsky, A. Szafer, C. Talmadge, and S. H. Aronson, Phys. Rev. Lett. 56, 3 (1986).
3. H. A. Chan, Ph.D. thesis, University of Maryland, College Park, Maryland (1982), unpublished.
4. E. R. Mapoles, Ph.D. thesis, Stanford University, Stanford, California (1981), unpublished.
5. H. J. Paik, J. Astronaut. Sci. 29, 1 (1981).
6. H. A. Chan, H. J. Paik, M. V. Moody and J. W. Parke, IEEE Trans. Magnetics, MAG-21, 411 (1985).
7. Model 330 RF SQUID system, Biomagnetic Technologies, Inc., San Diego, California.
8. Serafini and Koenig in Cryogenic Properties of Polymers.
9. E. J. Kramer and C. L. Bauer, Phy. Rev., 163, 407, (1967).

Table 1.

Pressure	C_C/C_B	C_M/C_B	τ_{BM}	τ_{CB}	τ_{MG}
$\approx 10^{-3}\mu$	0.73	0.60	8.3 s	0.46 s	5.24 s
20 μ	0.87	0.98	1.1 s	0.13 s	1.37 s
100 μ	0.47	1.5	0.99 s	0.43 s	0.69 s

Figure 1. Gradiometer

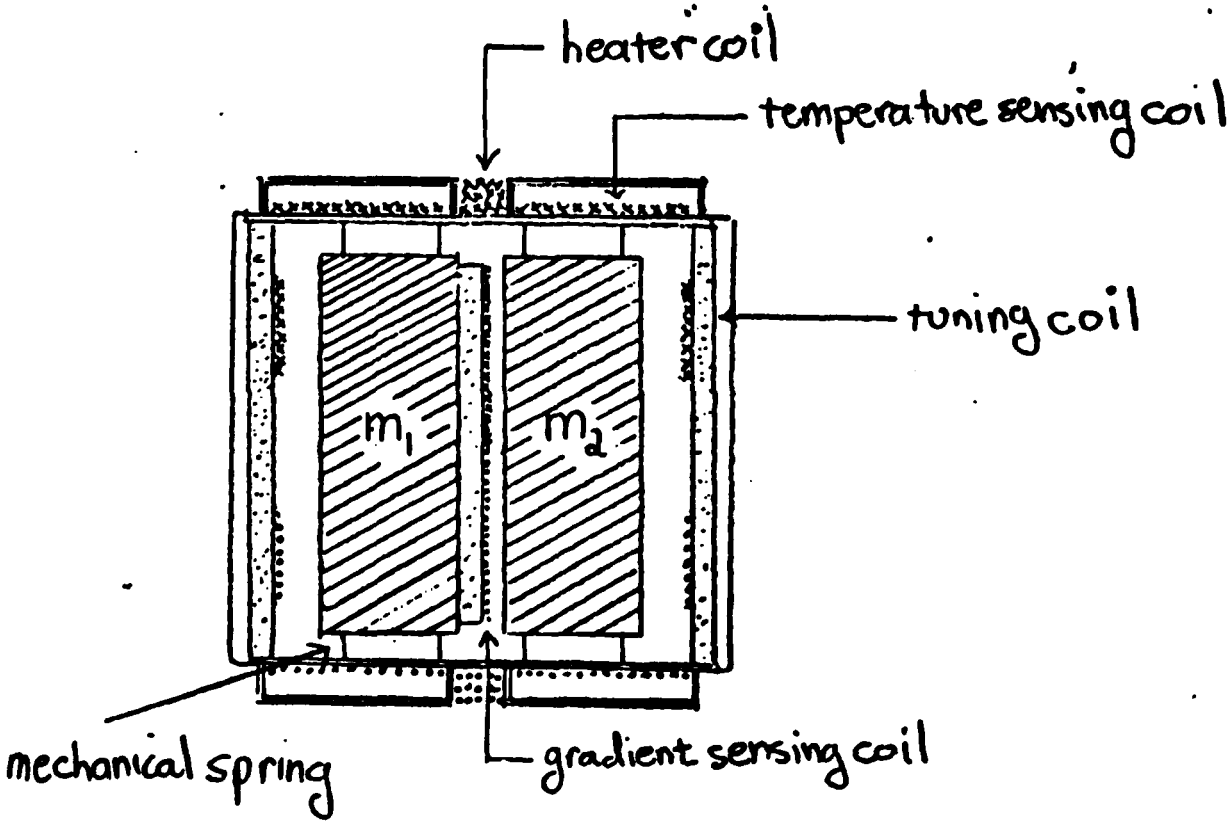

Figure 2 Readout Circuitry

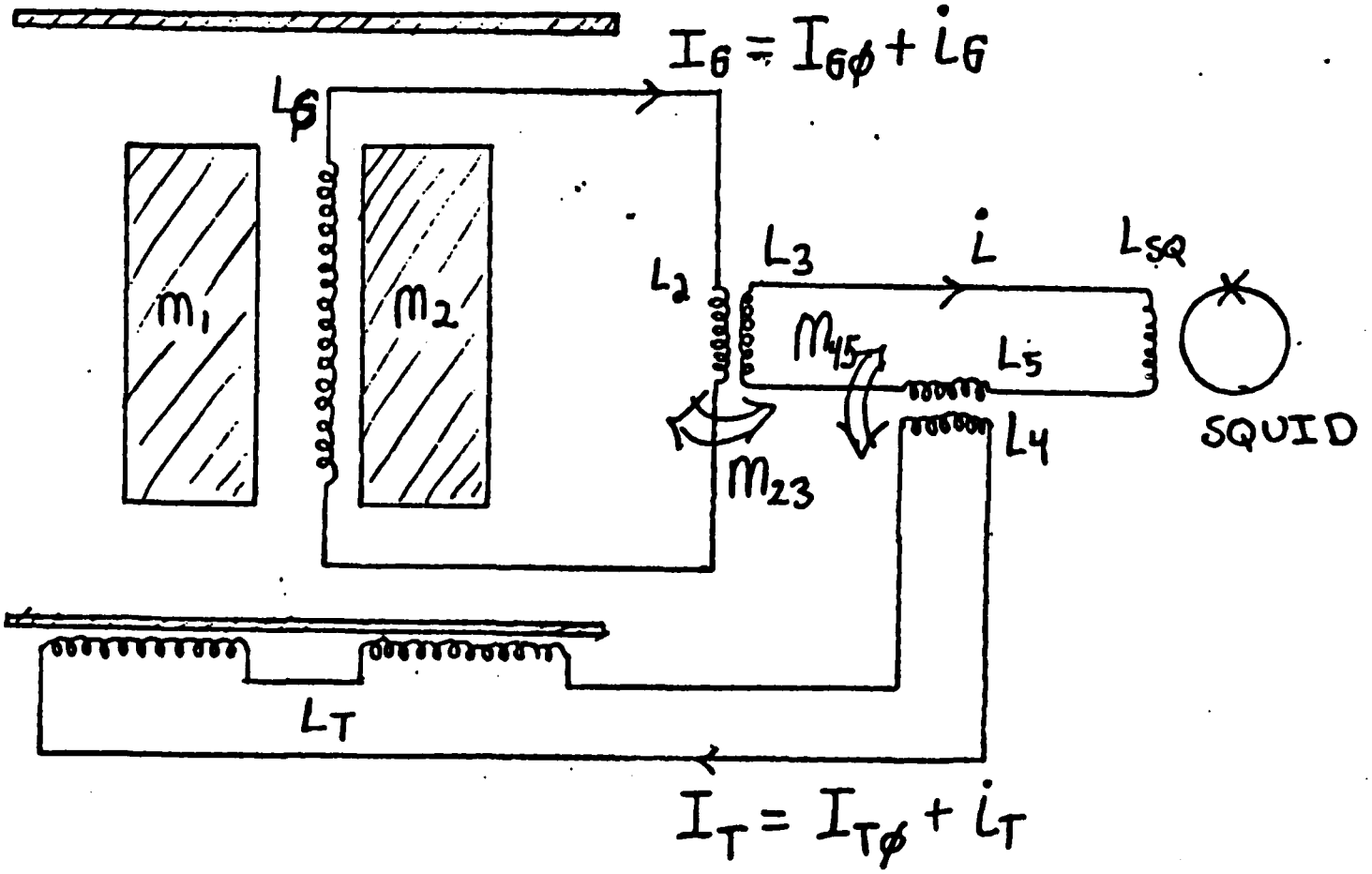

Figure 3 $f^2_{D,exp}$ vs I^2_{60}

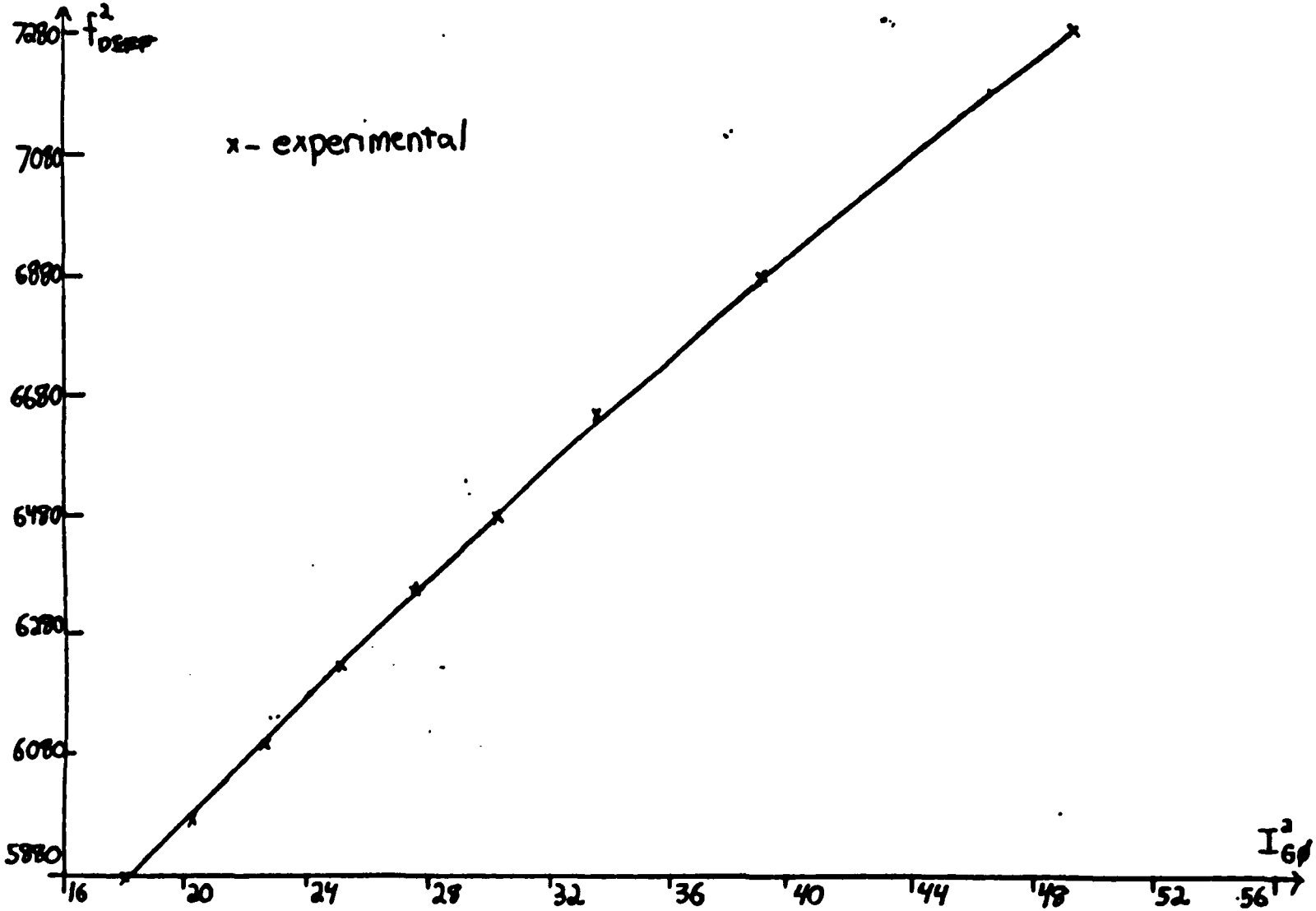

Figure 4

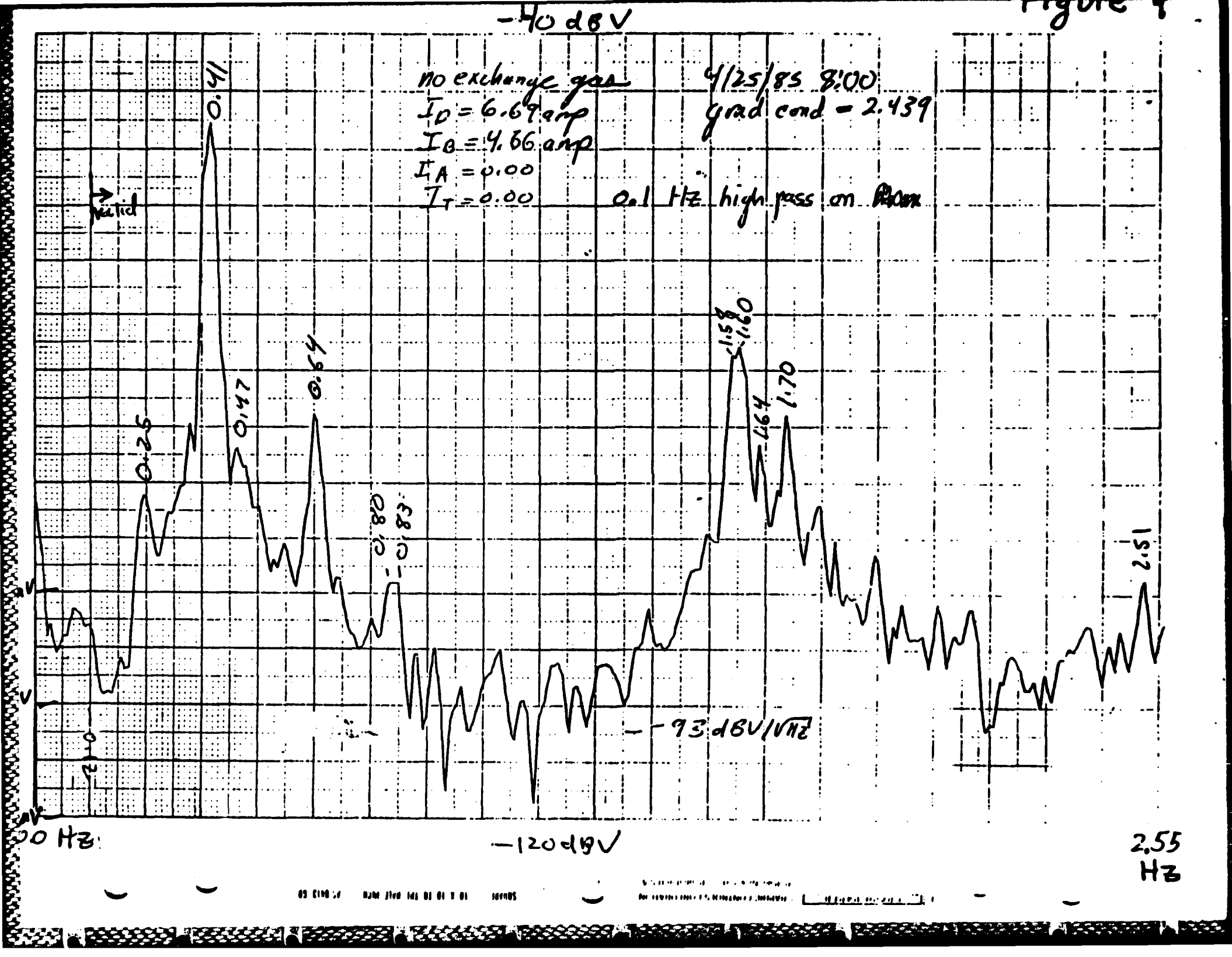
-40 dBV
no exchange gas
I_D = 6.69 amp
I_B = 4.86 amp
I_A = 0.00
I_T = 0.00
4/25/85 8:00
grad cond = 2.439
0.1 Hz high pass on Room
Initial
0.11
0.26
0.47
0.64
0.83
1.58
1.60
1.64
1.70
2.51
-93 dBV/√Hz
-120 dBV
2.55 Hz

Figure 5

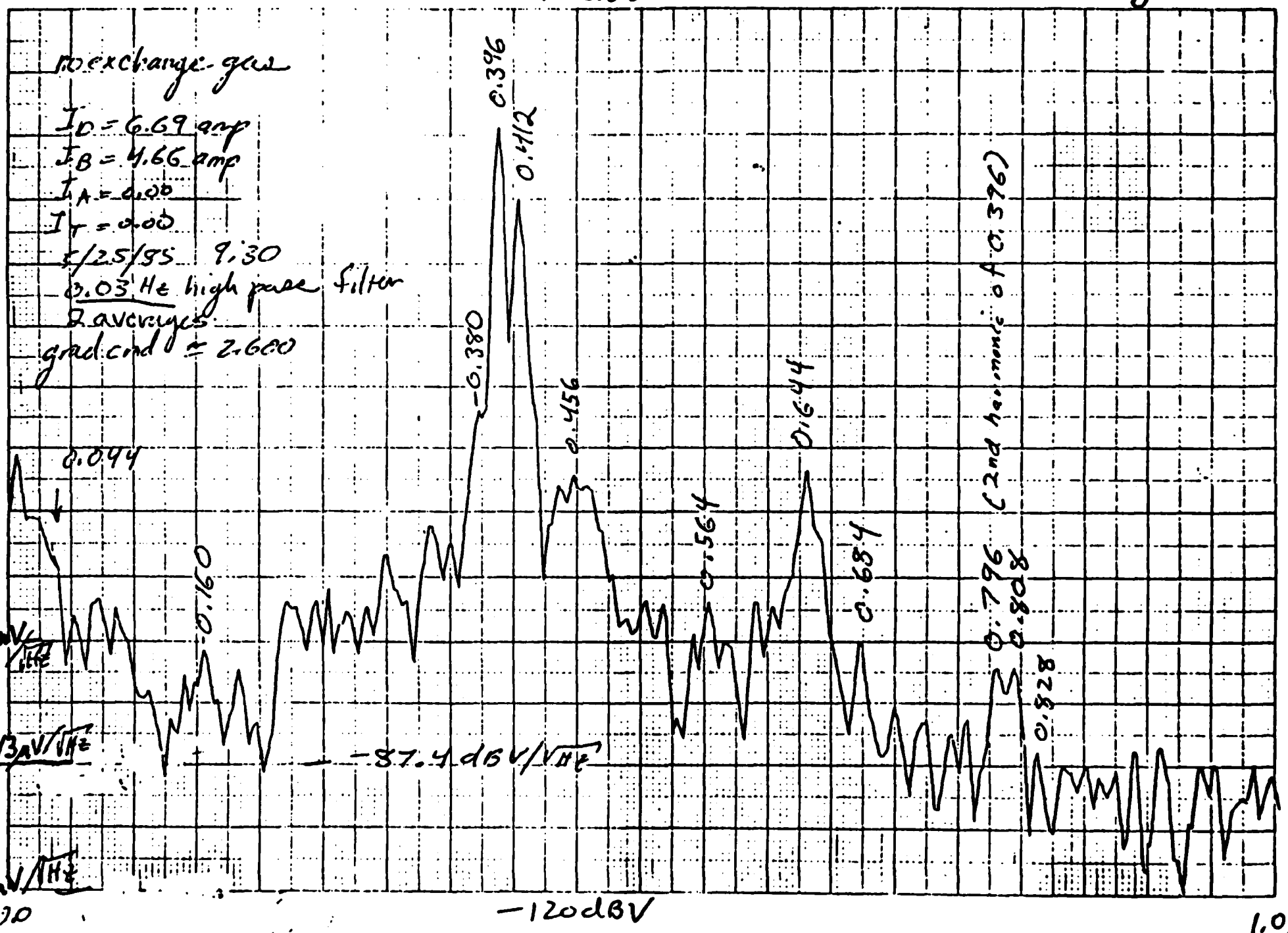
-40dBV
no exchange gas
I_D = 6.69 amp
I_B = 4.66 amp
I_A = 0.00
I_T = 0.00
2/25/85 9:30
0.03 Hz high pass filter
2 averages
grad cond = 2.600
0.044
0.160
0.380
0.396
0.112
0.456
0.564
0.644
0.684
0.796
0.808
0.528
(2nd harmonic of 0.396)
-87.4 dBV/√Hz
-120dBV
Hz
1,020
Hz

Figure 6

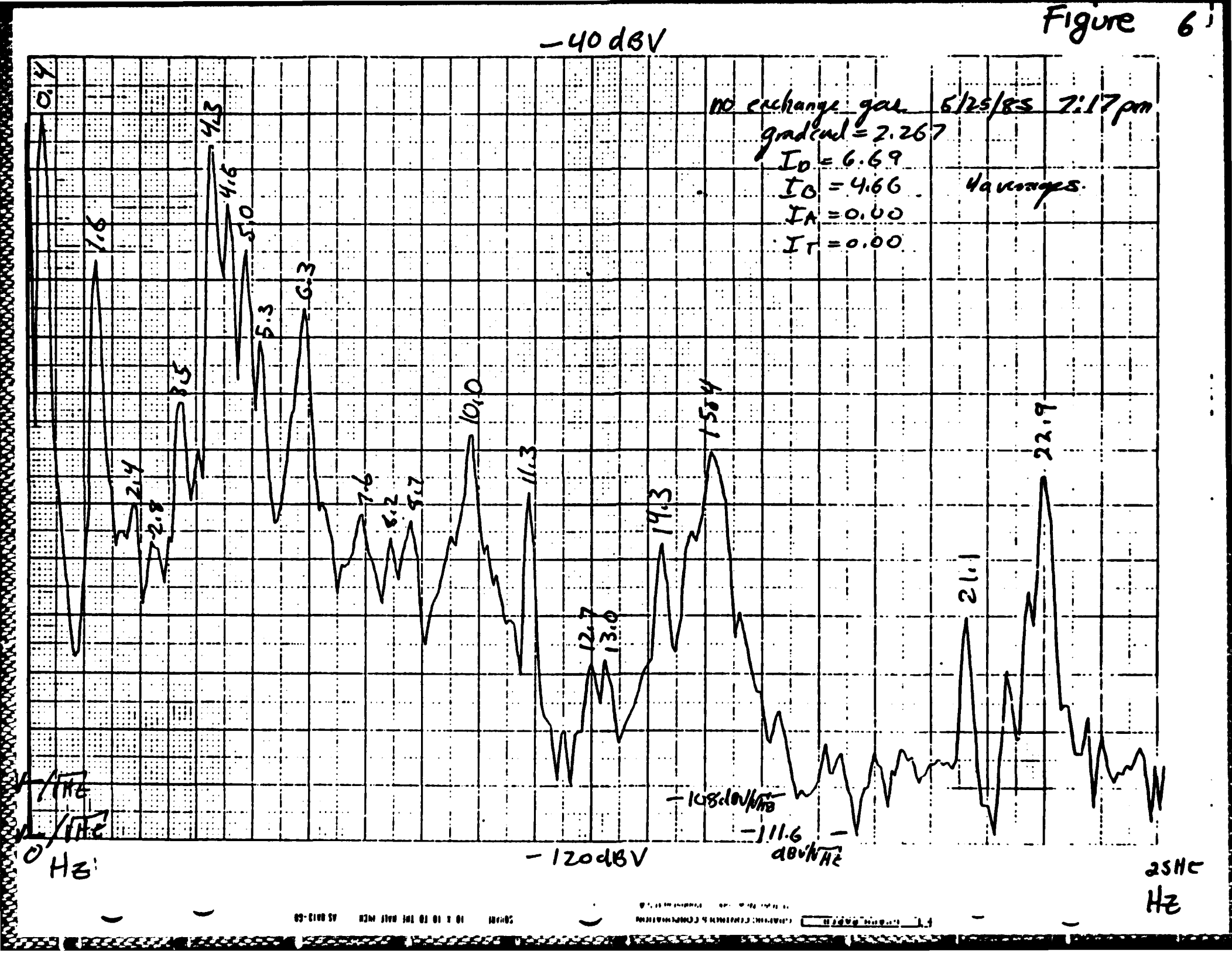
-40 dBV
no exchange gas 6/25/85 7:17 pm
gradient = 2.267
I_D = 6.69
I_D = 4.66 4 averages
I_A = 0.00
I_T = 0.00
0.4
1.6
2.4
2.8
3.5
4.3
4.6
5.0
5.3
6.3
7.6
8.2
8.7
10.0
11.3
12.7
13.0
14.3
15.4
21.1
22.9
-108.6 dBV/√Hz
-111.6 dBV/√Hz
-120 dBV
0 Hz
25Hz
Hz

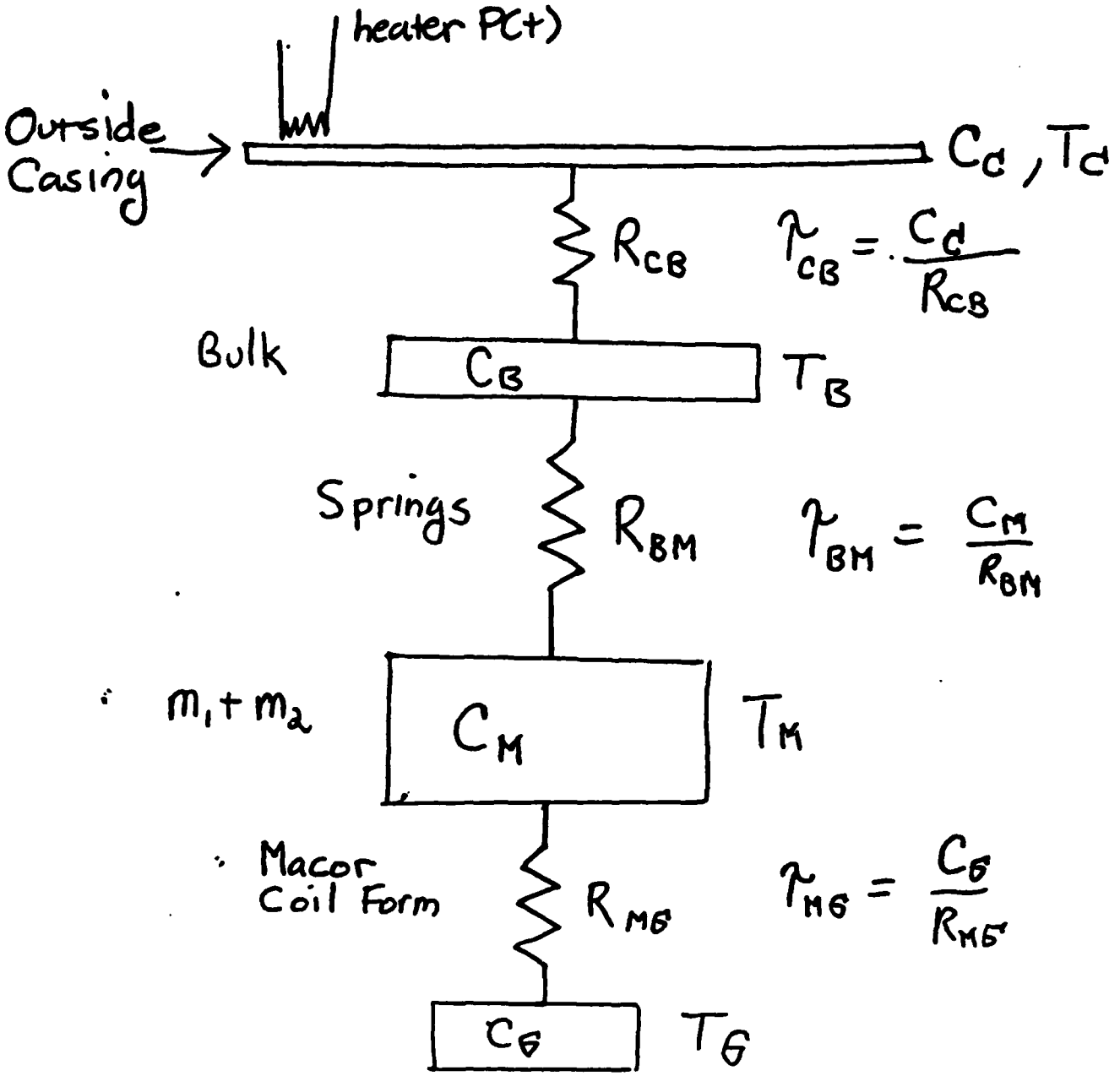

Figure 7 Thermal Model

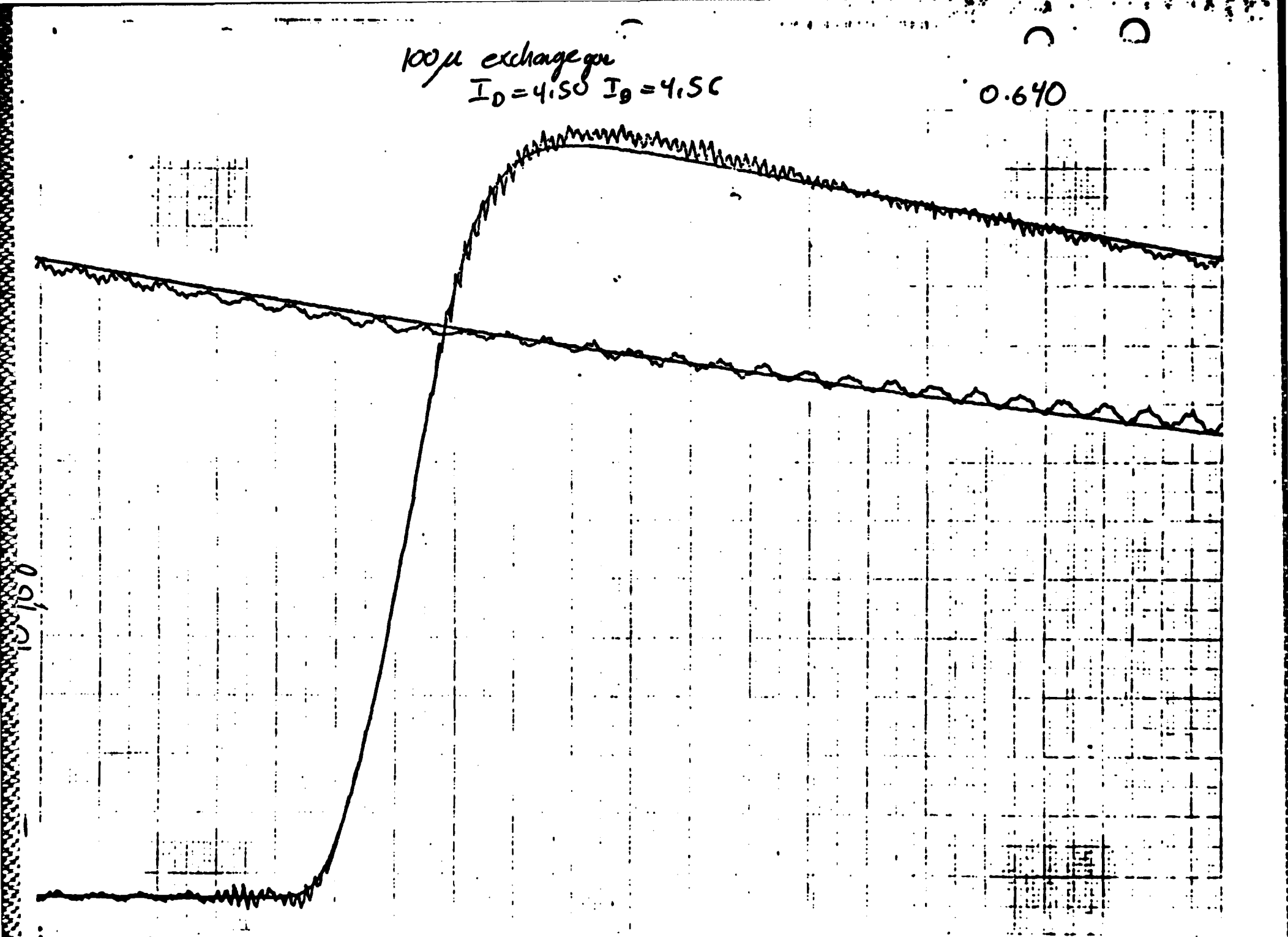

Figure 8 Gradient Sensing Circuit Impulse Response 256

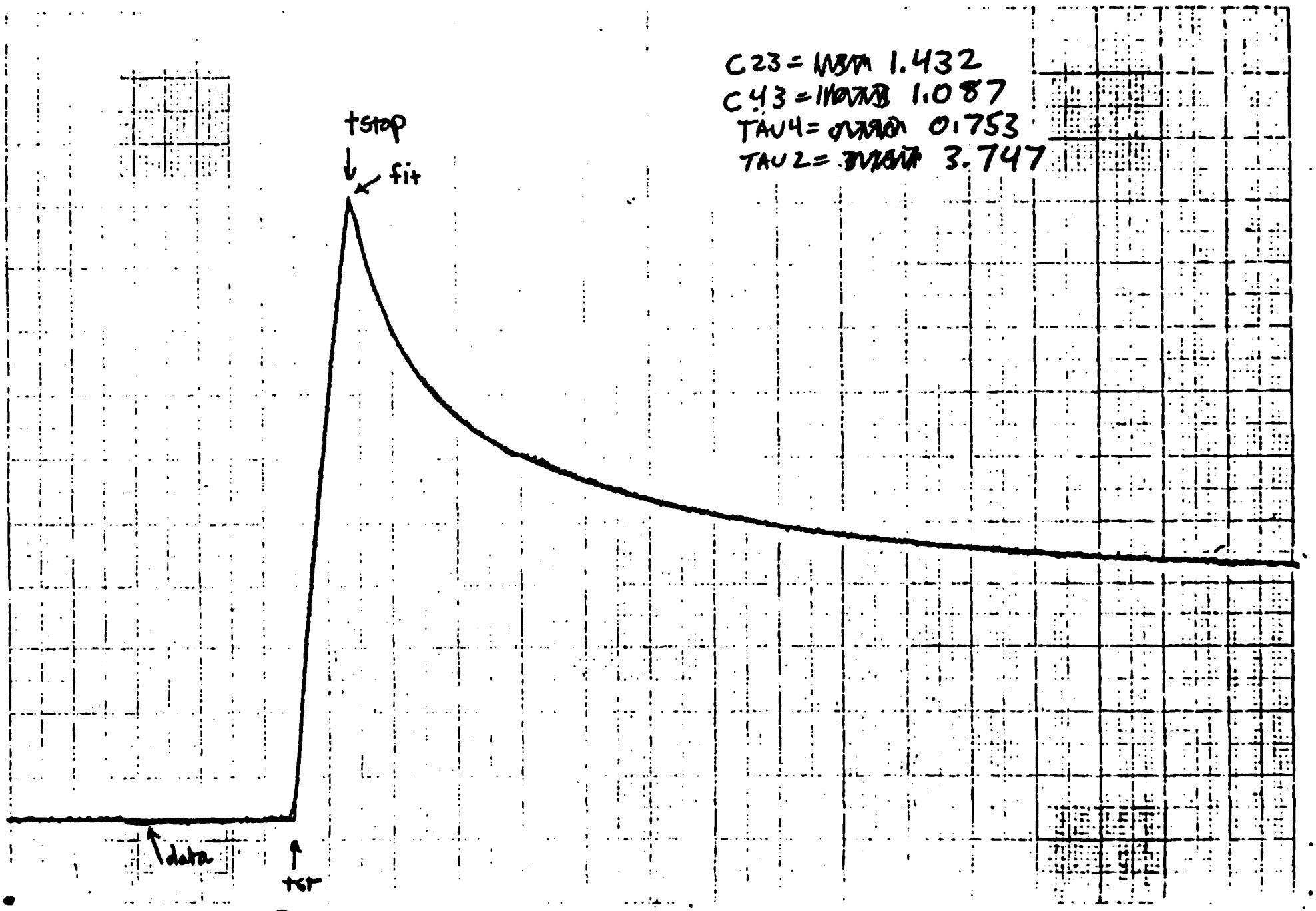

Figure 9 Temperature Sensing Circuit Impulse Response

Figure 10: $\frac{T_c - T_6}{T_d}$ amplitude and phase

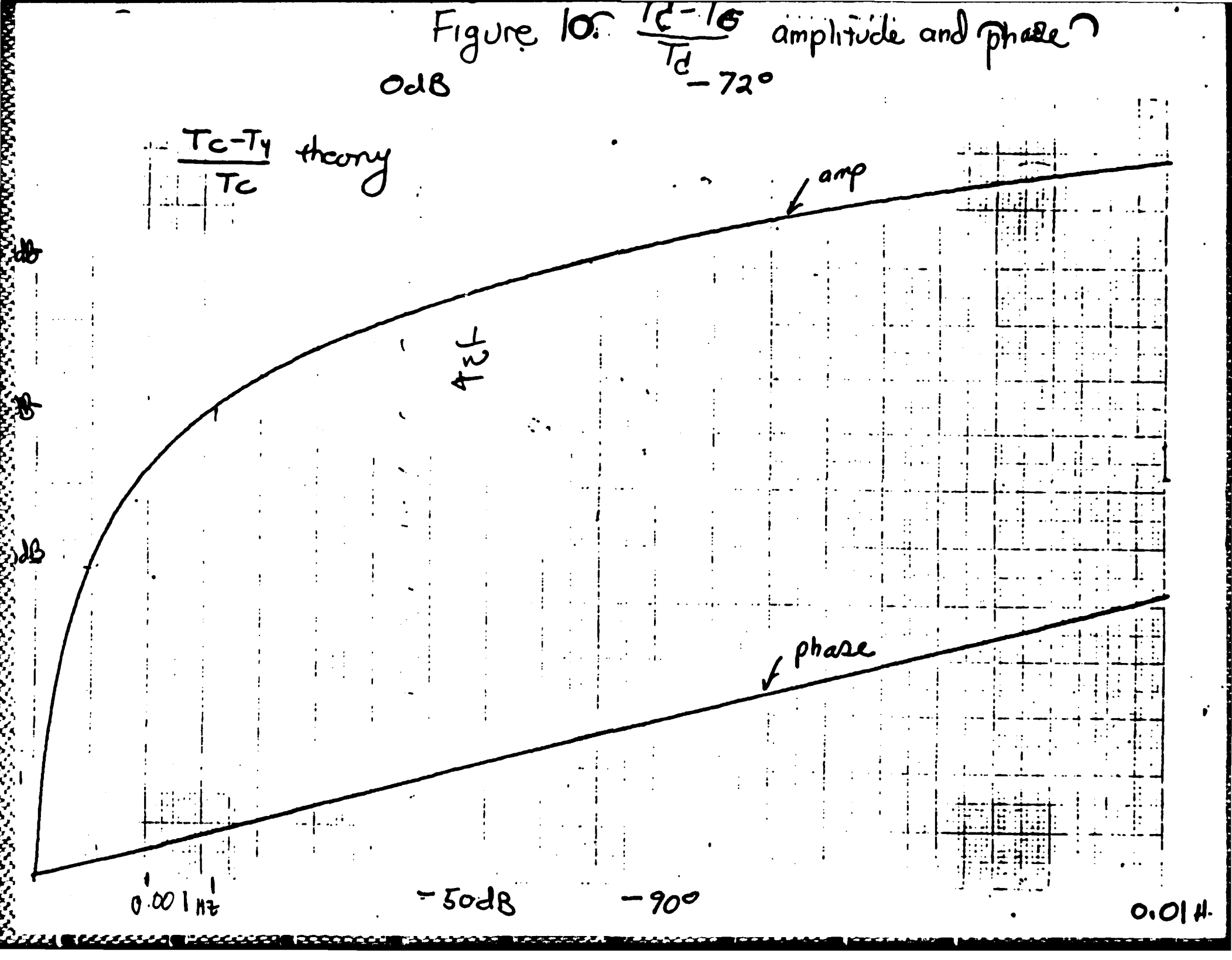

Figure 11 Temperature Sensitivity −50 dBV

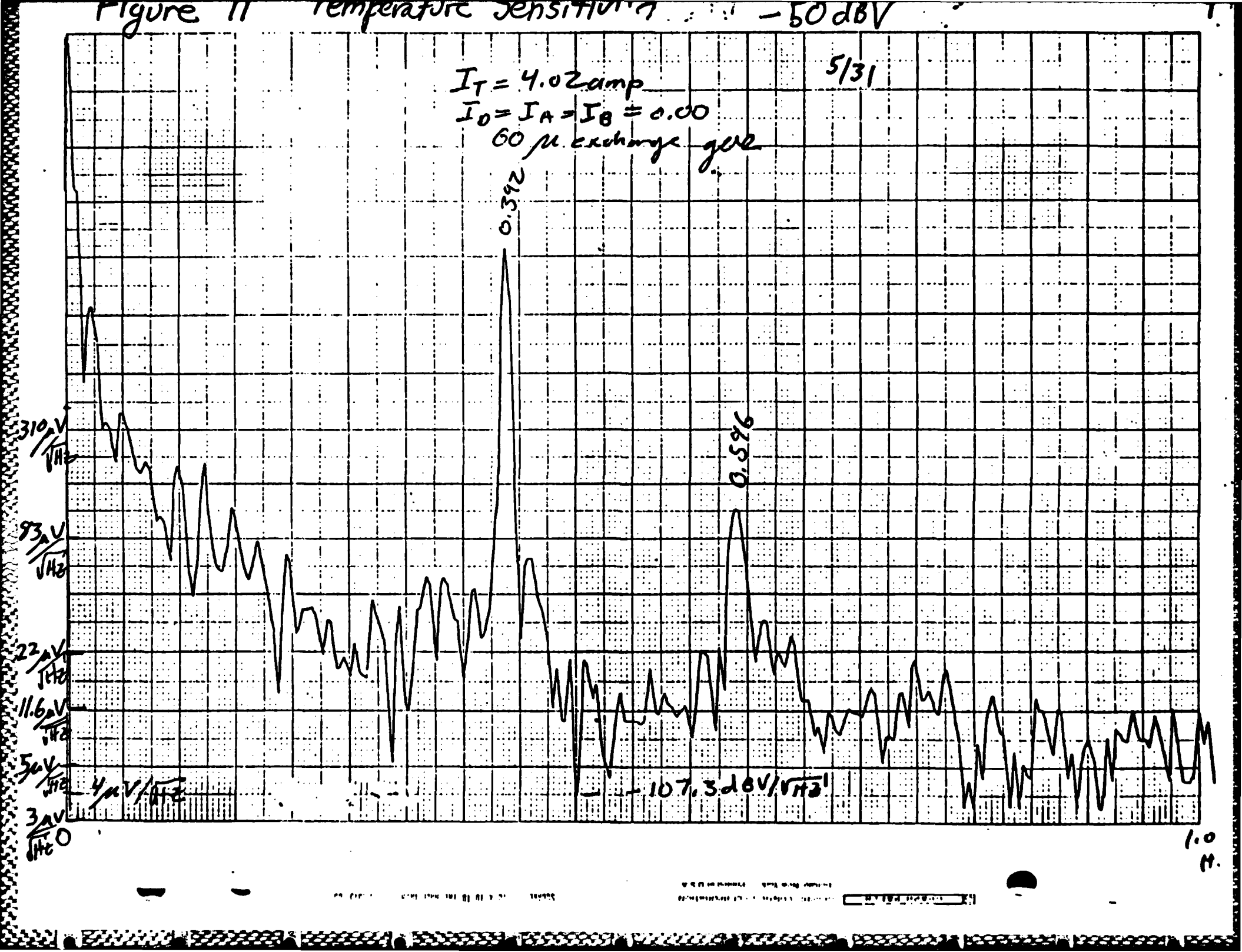

Comparison of Thermal noise to gradient Sensing Noise Figure 12

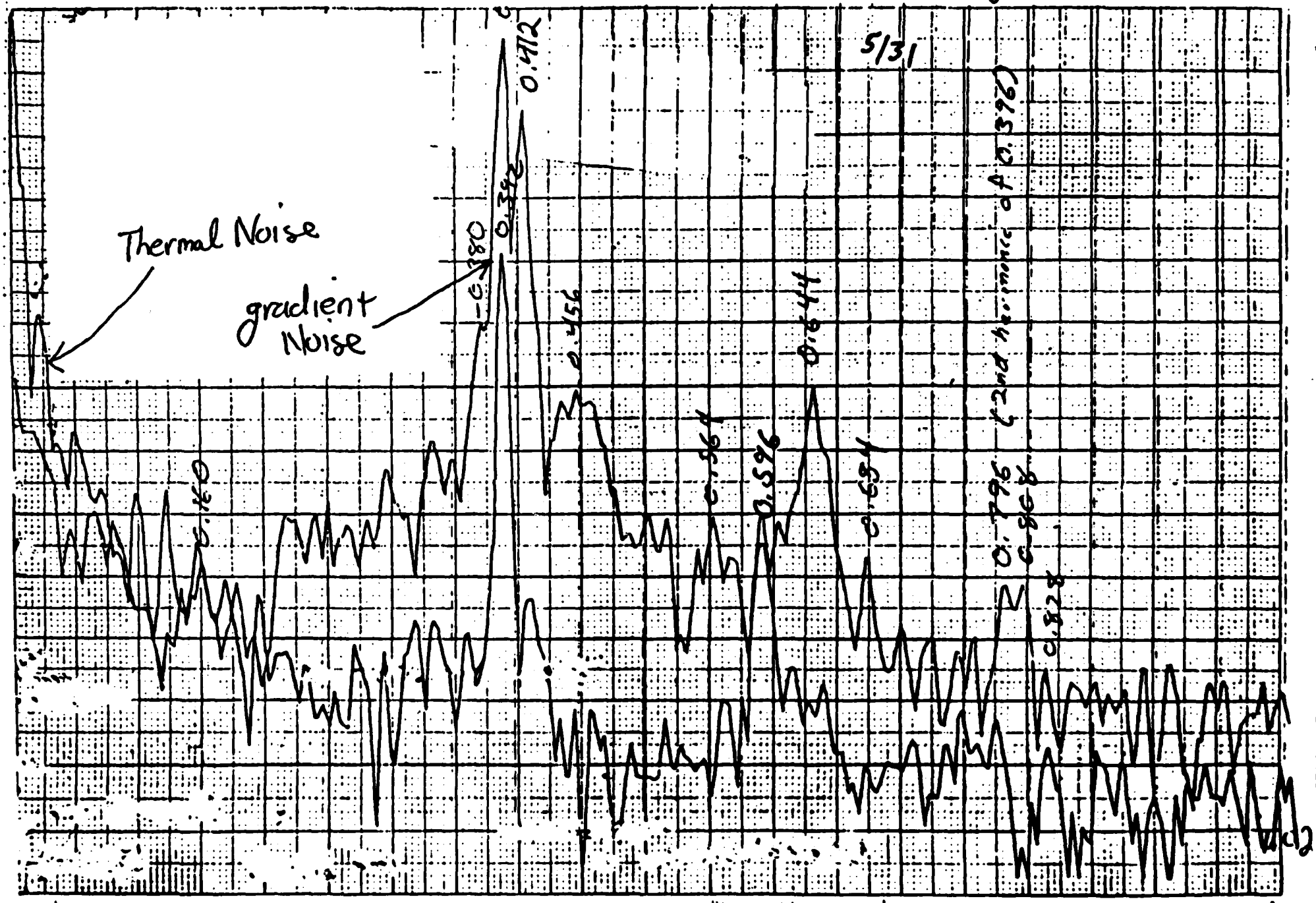

Figure 13 Seismic Activity of the Ground.

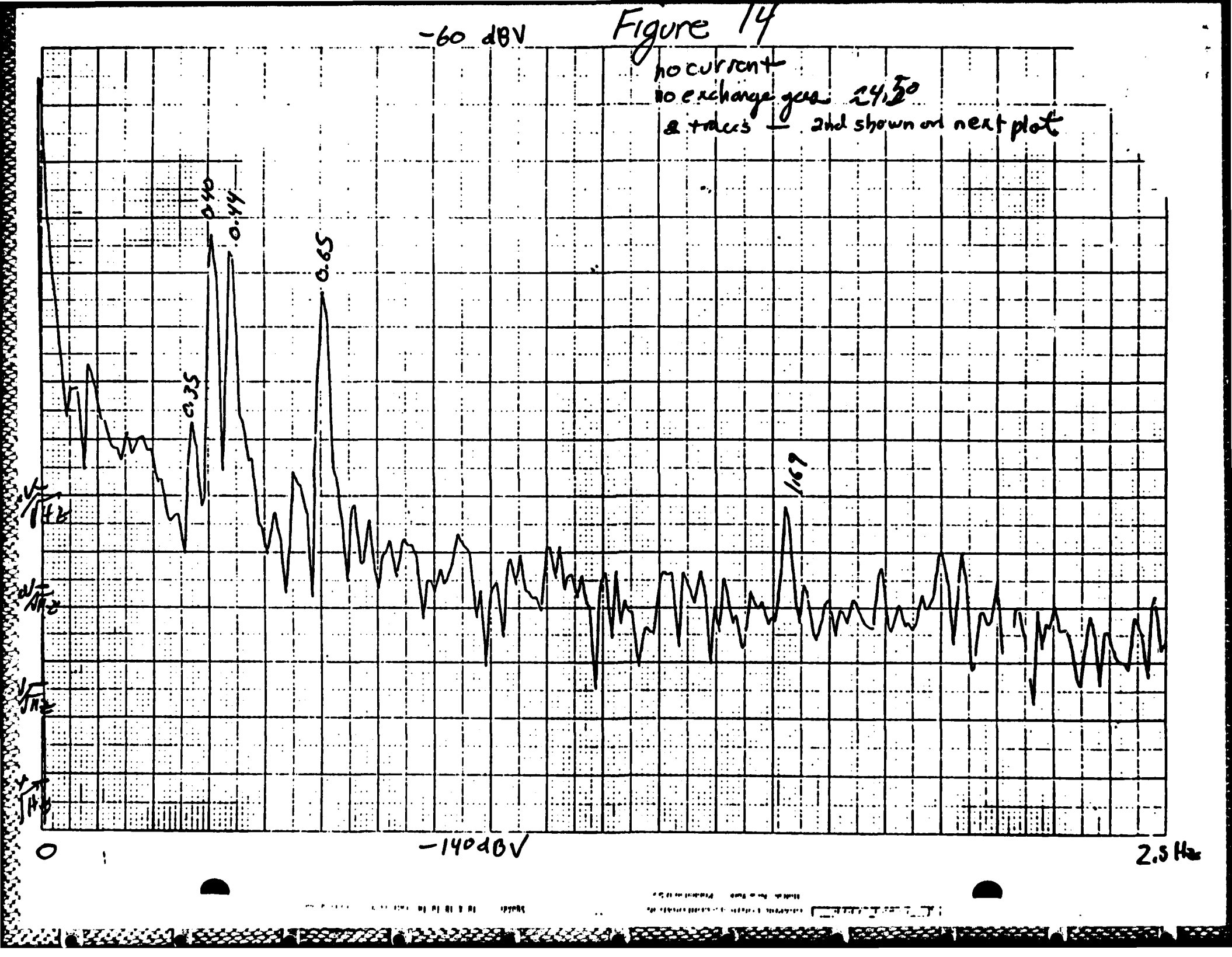
Figure 14
-60 dBV
no current
no exchange gas 24,30
2 traces — 2nd shown on next plot
0.40
0.44
0.65
0.35
1.69
-140 dBV
0
2.5 Hz

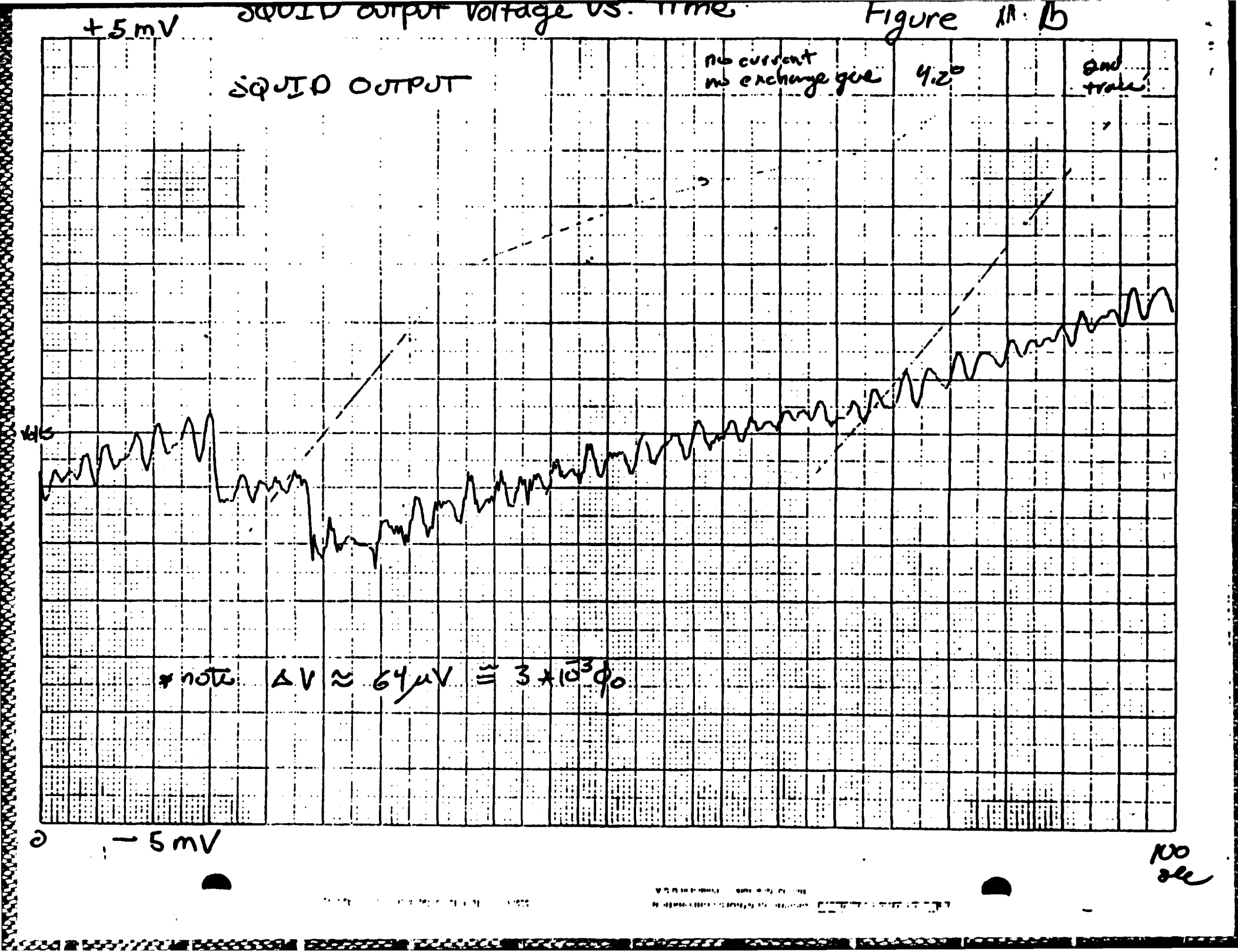
+5 mV
SQUID output voltage vs. time
Figure 11. b
SQUID OUTPUT
no current
no exchange gas
4.2°
and
trace
volts
* note ΔV ≈ 64 μV ≅ 3 * 10⁻³ φ₀
0
−5 mV
100
sec

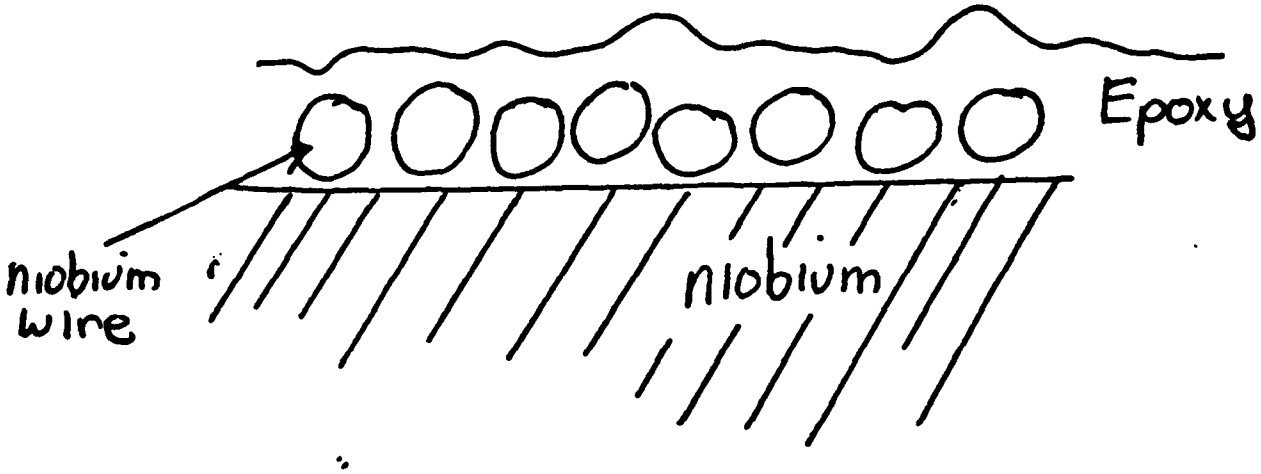

Figure 16 Temperature Sensing Coil

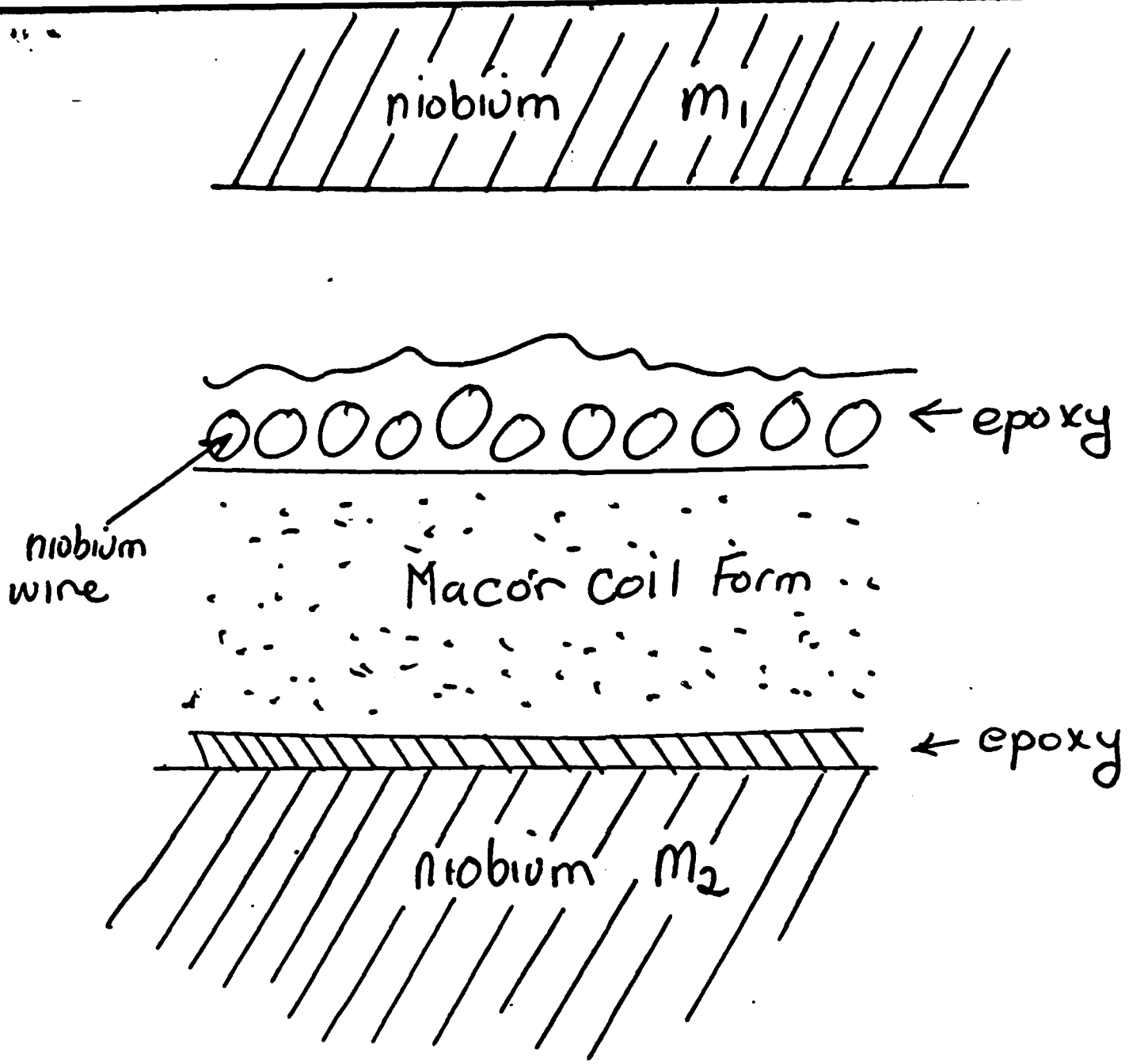

Figure 17 gradient sensing coil

END

9-87

DTIC